University of Texas at El Paso
ScholarWorks@UTEP

Open Access Theses & Dissertations

2022-12-01

Compact Electrospray Propulsion Systems For Small Form-Factor Satellites: An Orbital Performance Survey & Platform Design

Alberto Meza
University of Texas at El Paso

Follow this and additional works at: https://scholarworks.utep.edu/open_etd

 Part of the Aerospace Engineering Commons, and the Mechanical Engineering Commons

Recommended Citation

Meza, Alberto, "Compact Electrospray Propulsion Systems For Small Form-Factor Satellites: An Orbital Performance Survey & Platform Design" (2022). *Open Access Theses & Dissertations*. 3881.
https://scholarworks.utep.edu/open_etd/3881

This is brought to you for free and open access by ScholarWorks@UTEP. It has been accepted for inclusion in Open Access Theses & Dissertations by an authorized administrator of ScholarWorks@UTEP. For more information, please contact lweber@utep.edu.

COMPACT ELECTROSPRAY PROPULSION SYSTEMS FOR SMALL FORM-FACTOR SATELLITES: AN ORBITAL PERFORMANCE SURVEY & PLATFORM DESIGN

ALBERTO MEZA

Master's Program in Mechanical Engineering

APPROVED:

Amelia Greig, Ph.D., Chair

Angel Flores-Abad, Ph.D.

Jason Adams, Ph.D.

Mark Silver, Ph.D.

Stephen L. Crites, Jr., Ph.D.
Dean of the Graduate School

Copyright ©

by

Alberto Meza

2022

Dedication

I would like to dedicate this work to my parents and my brother for their relentless support throughout my education**.** And to Rowan, for being an indispensable, invaluable pillar throughout my graduate career.

COMPACT ELECTROSPRAY PROPULSION SYSTEMS FOR SMALL FORM-FACTOR SATELLITES: AN ORBITAL PERFORMANCE SURVEY & PLATFORM DESIGN

by

ALBERTO MEZA

THESIS

Presented to the Faculty of the Graduate School of

The University of Texas at El Paso

in Partial Fulfillment

of the Requirements

for the Degree of

MASTER OF SCIENCE

Department of Mechanical Engineering

THE UNIVERSITY OF TEXAS AT EL PASO

December 2022

Acknowledgements

I would first like to thank my advisor and mentor Dr. Amelia Greig for guidance not only throughout my graduate studies and research but for teaching me invaluable lessons that have allowed me to grow personally, academically and professionally. I am grateful to have taken part of outstanding research at UTEP's Aerospace center and for center to make these type of research opportunities possible to first generation minority graduate students. I'd like to thank my coworkers at the electrospray propulsion project for their work, determination and support to this project, without their contributions this project wouldn't be at the level it exists. Last but not least, I would like to thank Dr. Quintana, Dr. Adams and Arturo Reyes for their support, advice and their critical role in the development of skills that have formed me into becoming a better researcher and engineer.

Abstract

Over the past decades, small form-factor satellites such as CubeSats have remained as one of the most accessible platforms to reach space for universities, research institutions, private and governmental entities to perform a wide range of missions. This paper presents a survey into the design and implementation of an electrospray rail thruster, to be integrated to the CubeSat platform. The design investigated features propellant tanks for each individual thruster embedded inside the rail of a standard 1U CubeSat. The capabilities of utilizing the electrospray thruster as an attitude & determination control system was also investigated in which, a pointing accuracy study was created in order to compare the electrospray thruster to commercially available reaction wheels and magnetorquers compatible with the CubeSat platform. This study determined the minimum arcsecond each technology can achieve within 1 second of operation. Additionally, a mission capability survey was investigated to determine the capabilities of the electrospray thruster and platform, to perform a series of STK scenarios. The first STK scenario investigated the operational life extension of a 1U CubeSat by implementing an electrospray propulsion system with a combined thrust of 48μN compared to a 1U CubeSat with no propulsion. This study found that the 1U CubeSat with propulsion can increase its operational life up to 20 years during a solar minima period on a 500 km altitude initial orbit, and around 1.2 days for the case of the initial orbit of 250 km during a solar maxima period. Additionally, a GEO to Graveyard orbit transfer was investigated utilizing STK. This scenario utilizes the volume and mass of a standard 6U CubeSat with an electrospray propulsion system to perform an orbit change maneuver from an initial GEO orbit of 35,786 km in altitude, to a final graveyard orbit of 36,022 km in altitude within time window of 15 yrs. The study resulted in a total of 55 burn maneuvers, 5 hrs. in length each,

performed every 0.3 yrs. until successfully reaching the desired orbit within the 15 yrs time window.

Table of Contents

List of Tables

List of Figures

Nomenclature

ΔV	Change in velocity	km/s
a	Distance from center of mass to edge	m
a_a	Angular acceleration	°/s^2
a_d	Angular displacement	°
ADCS	Attitude and Determination control system	-
AERO VISTA	Aurora Emission Radio Observer and Vector Interferometry Space Technology using AERO	-
a_v	Angular velocity	°/s
B	Magnitude of local magnetic force	T
C_d	Atmospheric drag coefficient	-
CDS	CubeSat Design Revision	-
C_r	Solar reflection coefficient	-
d	Distance between extractor grid and tip	m
DoD	Department of Defense	-
E	Electric field	V/m
EET	Embedded Electrospray thruster	-
E_{tip}	Electric field at tip of emitter	V/m
GEO	Geostationary Orbit	-
g_o	Earth's local gravity	m/s^2
I	Moment of inertia	Kg•m^2
I_{sp}	Specific Impulse	s
j	Component normal to the surface of liquid	-

K	Electrical Conductivity Coefficient	-
LEO	Low-Earth Orbit	-
ln	Natural Logarithm	-
m	Mass	kg
m_i	Propellant mass after burn maneuver	kg
MIT	Massachusetts Institute of technology	-
M_m	Magnetic moment	$A \bullet m^2$
m_o	Initial propellant mass	kg
MPD	Magneto Plasma Dynamic Thrusters	-
NASA	National Aeronautics and Space Administration	-
NOAA	National Oceanic and Atmospheric Administration	-
P-POD	Poly-pico Satellite Orbital Deployer	-
PPT	Pulsed Plasma Thruster	-
R_c	Radius of curvature at the tip	m
STK	Systems Tool kit	-
SWaP	Size Weight and Power	-
t	time	s
UTEP	University of Texas at El Paso	-
v_e	Exhaust velocity	m/s
V_{start}	Start-up Voltage	V
γ	Liquid surface tension	N/m
ϵ_o	Permeability of free space	N/A^2
θ_i	Initial angular position	°

π	Ratio of a circle's circumference to its diameter	-
τ	Torque	N•m
ω_i	Initial angular velocity	°/s

Chapter 1 Heritage and Theory

1.1 Electric Propulsion Overview & Classifications

At present, a demand for more complex spacecraft and satellite missions has contributed to the densification and advancement of new electric propulsion technologies. This technology sees its roots since 1960s when NASA's SERT-I, an ion thruster, successfully demonstrated flight capabilities to perform station keeping maneuvers, orbit insertions as well as primary being employed for primary propulsion systems for deep space missions [1]. It wasn't until the 1980s that electric propulsion saw its first commercial use, with the Intel Sat V2, a Ford Aerospace's communication satellite which was launched and saw success in its operation of a resistojet thruster [2]. As deliberated by chemical propulsion systems, electric propulsion systems are also bounded by the same equations such as Tsiolkovsky's ideal rocket equation to characterize and analyze a variety of performance parameters:

$$\Delta V = v_e \, ln \frac{m_o}{m_i} \tag{1.1}$$

where ΔV refers to the velocity increment, $\boldsymbol{v_e}$ is the exhaust velocity of the propellant and $\frac{m_o}{m_i}$ is the mass fraction between the initial mass of the system and the mass after performing a burn maneuver. Furthermore, another metric utilized to characterize performance known as specific impulse I_{sp} can be described as:

$$I_{sp} = \frac{v_e}{g_o} \tag{1.2}$$

where $\boldsymbol{g_o}$ refers to standard earth gravity. Electric propulsion typically characterized by the type of fuel being used which can be liquid or solid, and by the integration of an electrical source. Over the past decades numerous publications aiming at compiling the many different branches electric propulsion denote three main categories of its own, which are electrostatic,

electrothermal and electromagnetic [3, 4, 5]. Electrostatic propulsion systems utilize their electric source to ionize their fuel where ideally, ions are accelerated via the application of an induced electric field. The thrusters contained in this category includes: Electrospray & gridded ion. Electrothermal shares similarities to similar concepts from chemical propulsion in which electricity becomes the source to heat the propellant in a chamber where expanded heated gas accelerates through a nozzle. Thrusters found on this category include arcjet and resistojets. Electromagnetic propulsion involves the use of both electric and magnetic forces to accelerate ionized particles. Thrusters that share the characteristics of this category include: Pulsed plasma thrusters (PPT), magneto plasma dynamic thrusters (MPD) and Hall effect thrusters.

1.2 ELECTROSPRAY PROPULSION THEORY

Electrospray propulsion being under the category of electrostatic propulsion, consists on the use of an ionic propellant that is electrically charged. The induced electric field ionizes the propellant, and accelerates positively charged particles, thus creating thrust. Traditionally electrospray thrusters consist on a propellant tank, a porous media, and extractor grid and a power source. The Massachusetts Institute of Technology aerospace department has vastly contributed to the characterization of the fundamental dominating forces acting upon these types of thrusters. The equations derived not only describe the physics and science behind electrospray thrusters but they also serve as useful tools to obtain critical design paramters that fundamentally affect the desired capabilities of the thruster itself [6].

$$E_{tip} = -\frac{2V/R_c}{ln(\frac{4d}{R_c})} \tag{1.3}$$

$$\frac{1}{2}\epsilon_o E_{tip}^2 > \frac{2\gamma}{R_c} \tag{1.4}$$

Equation 1.4 describes an inequality equation between the electrostatic forces created by the induced electric field, and the surface tension forces between the ionic liquid and the porous media. Where $\boldsymbol{\epsilon_o}$ is the permeability of free space, E_{tip} is the electric field at the tip of a single emitter, $\boldsymbol{\gamma}$ is the surface tension of the liquid and R_c is the radius of curvature of the tips. Rearranging equation 1.3 & 1.4 yields equation 1.5 for the start-up voltage which is defined by the minimum voltage required for emission to occur.

$$V_{start} = \sqrt{\frac{\gamma R_c}{\epsilon_o}} ln\left(\frac{4d}{R_c}\right) \tag{1.5}$$

A characteristic of achieving startup voltage on electrostatic devices is the formation of a peculiar phenomenon denominated as a Taylor Cone [7].

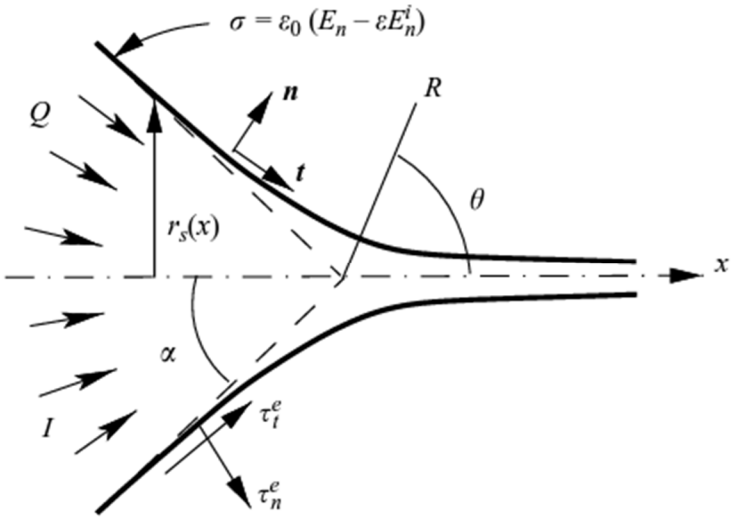

Figure 1 Sketch of the cone-to-jet transition region [7].

Where τ' is the mean curvature of the surface, λ is the surface tension of the liquid, ε_o is the permeability of free space, σ is the density of free charge at the surface of the liquid. By inducing

a dielectric field between the ionic liquid and the extractor grid, density of current the ionic propellant in the propellant creates a conduction current $\boldsymbol{j} = \boldsymbol{KE^i}$ where $\boldsymbol{K}$ is the electrical conductivity coefficient of the liquid, and $\boldsymbol{j}$ is the component normal to the surface of the ionic liquid, accumulating charge which is then convected by the flow [8].

Chapter 2 Platform Design for Embedded Electrospray Propulsion System

2.1 1U CubeSat Platform

Over the course of the past decades, CubeSats have remained as popular platform for academia, private industry and federal organizations to learn, conduct research, perform technology demonstration missions in a cheaper and faster process, in contrast with other satellite size categories.

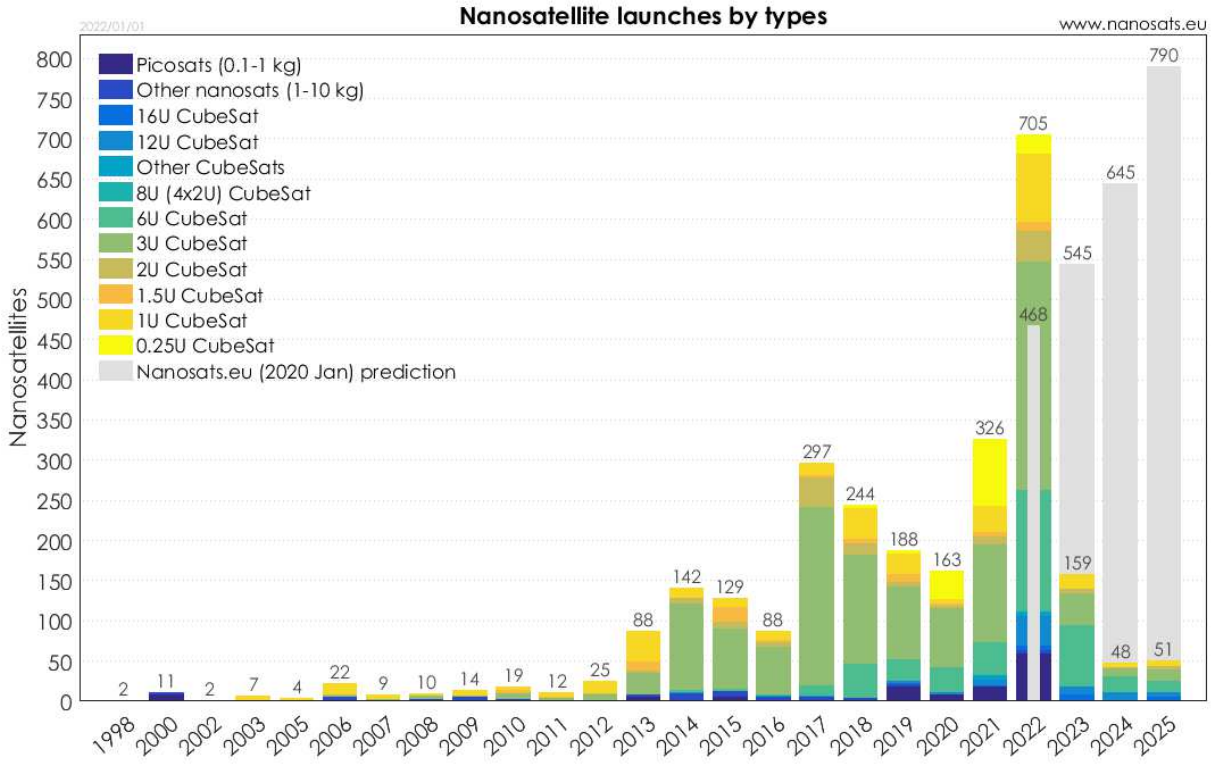

Figure 2: CubeSat Launches per Type [9].

Since 2003, a significant increase of CubeSat launches has been recorded, 1663 CubeSats being launched as of January 1st 2022[9]. Inevitably, utilizing the CubeSat platform comes with constrains and downsides of its own, in which the limitations include limited; available mass and volume payload, longevity of its missions, maneuverability and propulsion systems. CubeSats

have been developed by the California Polytechnic State University, where the CubeSat Design Specification (CDS) documentation defines its constraints and requirements that a CubeSat is composed of. Following the latest CDS revision 14, some of the characteristics which defines a 1U CubeSat includes a maximum mass of 2 kg and a volume of 10 cm x 10cm x 11.3 cm[10].

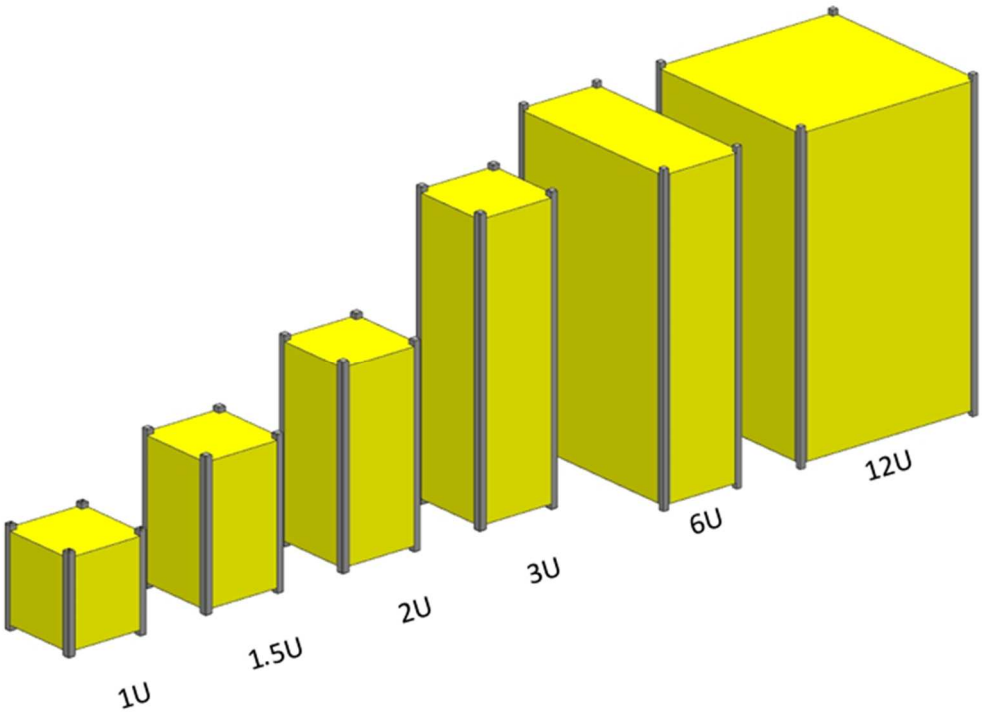

Figure 3: Current CubeSat Family [10].

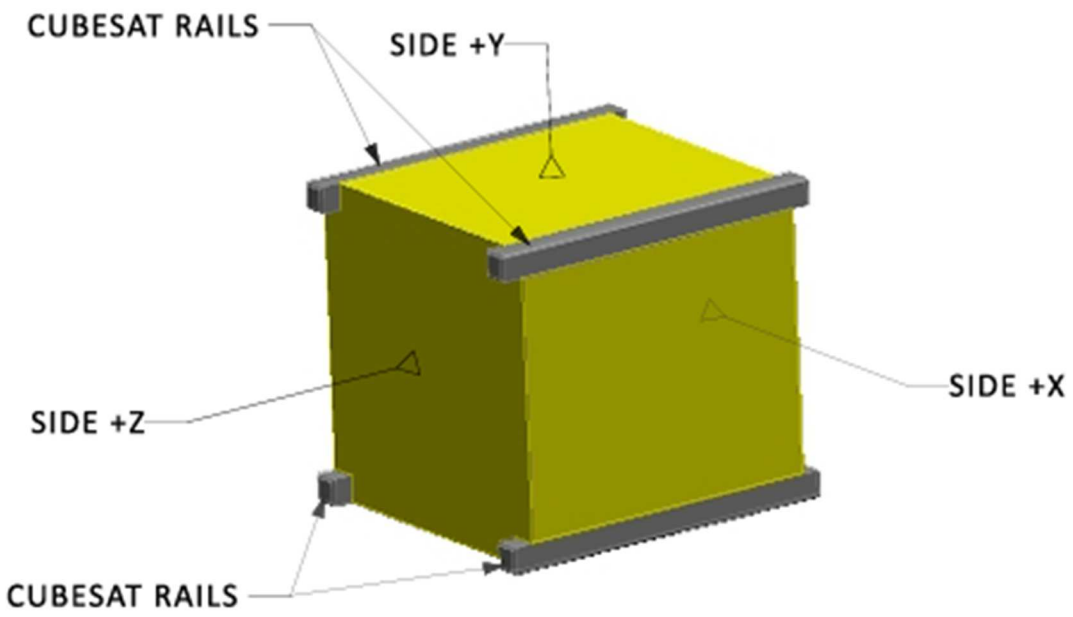

Figure 4: 1U CubeSat Specification Drawing [10].

2.2 Integrating Electrospray Thrusters to the CubeSat Platform

At the University of Texas at El Paso's Aerospace Center, electrospray propulsion technology for small form-factor satellites has been investigated [11]. This electrospray thruster is composed of a 216-hole stainless-steel extractor grid, a porous glass emitter array featuring 216 emitter tips, ground plate, an insulating casing and the propellant reservoir. By utilizing the electrospray thruster design previously discussed, this paper will investigate the implementation of an electrospray thruster for a standard 1U CubeSat platform.

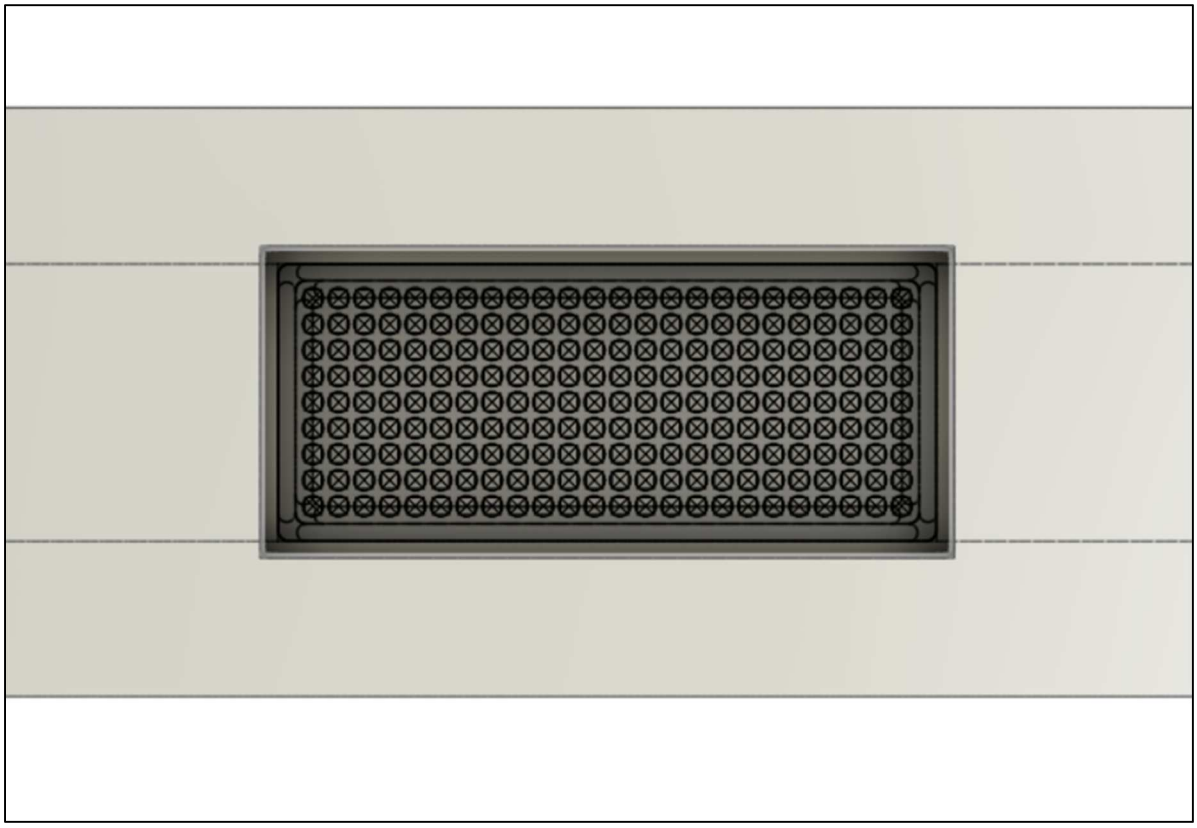

Figure 5: Electrospray thruster integrated to rail section CAD (close-up).

As minimizing the Size, Weight and Power Consumption (SWaP), remains as main focus and theme for the platform design, the structure of the CubeSat which on its mainly, its composed of rail sections will be employed as the common work ground for the integration of the electrospray thrusters. For this design, rail sections of the CubeSat platform are utilized for both the fuel tanks for the ionic liquid, and the thruster body, all of this within the dimension's constraints found int CDS revision 14.

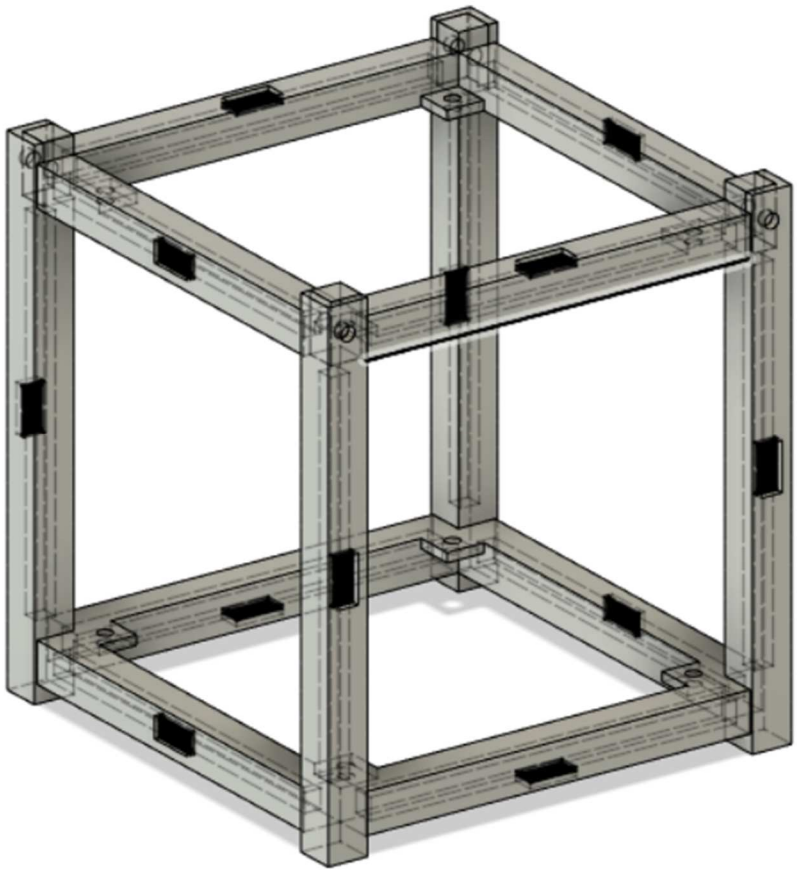

Figure 6: CAD model of a 12-Thruster Configuration for a 1U CubeSat with hidden edges (Isometric view).

As shown in the CAD model displayed on figure 4, the 12-thruster configuration for a 1U CubeSat utilizes every rail of the CubeSat structure without repeating thruster placement for an individual rail. Limiting a thruster to be installed in an individual rail allows the thruster to have its own independent fuel tank without the need to be shared with multiple thrusters, thus maximum fuel mass consumed can be determine per thruster basis.

Table 1: Rail tank parameters for 12-electrospray thruster configuration

Parameter	**Unit**	**Value**
Tank Volume	m^3	0.000019197

Maximum Fuel Mass	kg	0.0238
Ionic liquid Density	kg/m^3	1240

Following CDS revision 14, for a CubeSat to be compatible with a variety of dispensers, CubeSats must avoid any protrusions along rails or faces, since they can become point of failure when deploying, due to the interferences that can be created between the sliding rails from the dispensers and the CubeSat surfaces.

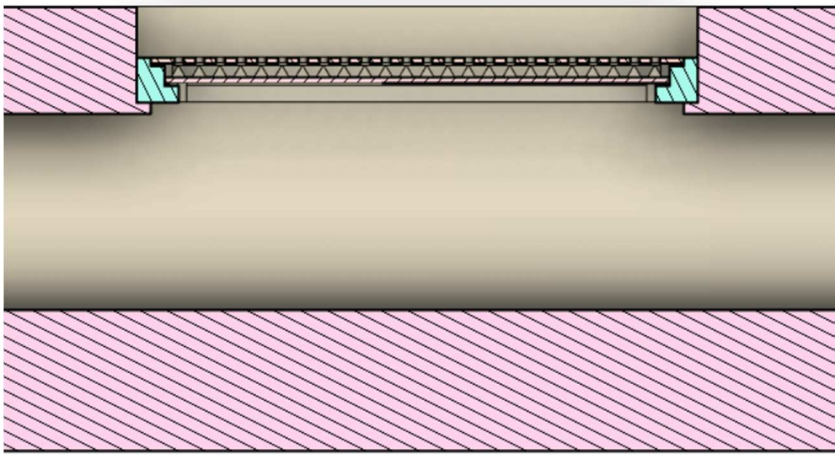

Figure 7: Rail tank & Thruster CAD Cross section.

As seen on Figure 3, small fixed steps are created to support the porous glass emitter array and the stainless-steel extractor grid which sits on top of it. The current thruster configuration in subject allows for the CubeSat to conduct burn maneuvers to provide linear thrust for 3-axis translation, and also by alternating opposite thrusters to allow 3-axis rotation for a total of 6 degrees of freedom.

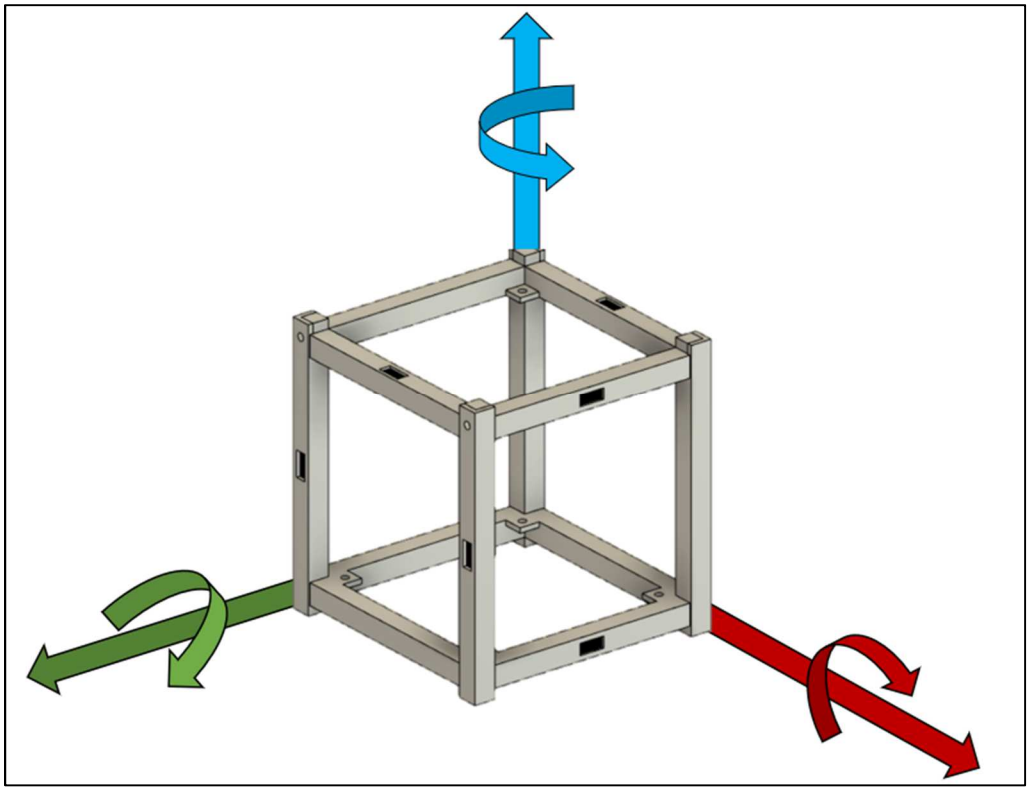

Figure 8: 1U CubeSat with 6 Degrees of Freedom.

A 12-thruster configuration (seen on figure 8) occupies the maximum amount of thruster per rail could also be used to extend the ΔV along the positive velocity vector of the satellite's orbit. This could be achieved by allocating propellant mass to perform small rotating maneuvers, effectively switching the desired thruster face to align with the positive velocity vector of the satellite and utilize the propellant and thrust from a different pair of thrusters allocate on other faces of the CubeSat platform.

Chapter 3 Orbital Capabilities Analysis

3.1 CubeSat Missions Survey

CubeSats have become an alternative platform allowing their users access to space in a faster and less expensive manner. Adding on, their low cost, weight and simple integration to mission architecture allows CubeSat to be assigned as secondary payloads or rideshares. Standardized dispensers known as P-PODs deployment mechanisms allow CubeSats to be deployed to numerous orbits and destinations [12]. Over the years, CubeSats have demonstrated capability to carry out a range of applications including telecommunications, technology demonstration missions, spaceborne & earth science observations, astrophysics, and potential deep space missions with the upcoming NASA's Artemis program. Interest in low-cost CubeSat telecommunication constellations in LEO has been shown from Department of Defense (DoD), federal entities, and private industry. As technology densifies it is required for CubeSats to achieve higher downlink rates which directly limits the payload's capability to transmit data to its user [12]. Among the astrophysics applications, ASTERIA, a conjoined effort between NASA's Jet Propulsion Laboratory and MIT has culminated in a scientific mission with the goal of studying exoplanet via a 6U CubeSat platform, utilizing the transfer method [13]. On the light of potential environmental treats that will impact the everyday life of the common person, earth Science observation missions aim to extend our current understanding of our very own planet by studying the oceans, ice caps, weather patterns, natural disasters, atmospheric composition and even to study Earth's auroras as it will be the case for the upcoming AERO VISTA Mission. As is currently under development by MIT Lincoln Laboratories, MIT, Morehead State University, MIT Haystack Observatory, AERO VISTA consists of two 6U twin CubeSats that will help provide more insight into the evolution of auroral emission features [14].

3.2 ATTITUDE DETERMINATION & CONTROL SYSTEMS FOR CUBESATS

During the early stages of the pico-satellite era, limited control and maneuverability of CubeSats would result in purposely allowing the spacecraft to tumble around in orbit as they conduct and achieve mission objectives, after which, naturally deorbiting and disintegrating in the atmosphere, bringing an end to its operational life. As for any satellite or spacecraft, propulsion systems and Attitude Determination and Control Systems extend the range of missions that can be performed, among these attained capabilities it includes; orbit transfers and corrections, station keeping maneuvers, operational life extension, high accuracy pointing maneuvers, de-orbit maneuvers, among others. Due to SWaP considerations, in order to integrate propulsion systems for small satellite form-factors such as CubeSats, the commercial availability and selection and diversity remains relatively limited in contrast to the available more mature options for medium to big form-factor satellites. Over the past years, numerous efforts have been conducted in order to monitor and keep track of propulsion systems for CubeSats with flight heritage [15, 16]. Flight proven categories of propulsion systems for CubeSats include cold gas, electrothermal, electrodynamic, electrostatic with the exception of chemical propulsion system in which their concepts are still on stand by for their respective demonstration missions.

Traditionally, Attitude Determination a Control Systems often rely on the use of reaction wheels and magnetorquers to perform a variety of maneuvers such as pointing instruments, detumbling maneuvers after P-POD ejection. Today, a significant number of commercial options of reaction wheels and magnetorquers for CubeSat platform exist in a variety of configurations allowing the user to tailor to its application. An example for commercially available reaction wheels for CubeSat can be seen on Rocket Lab's space systems reaction wheel line of products, with their

smallest reaction wheel achieving minimum angular momentum of 0.003 Nms with a mass of less than 50 g and a volume of 33.5 x 33.5 x 17 mm, and their largest option achieving a minimum angular momentum of 1 Nms, with a mass of 1390 g and a volume of 154 mm x 146 mm x 45 mm [17].

3.3 Pointing Accuracy Study

Utilizing the expected thrust for the second-generation rail thruster currently under development by the UTEP's Aerospace Center, a pointing accuracy study has been investigated in which performance parameters of the selected magnetorquers and reaction wheels were compiled and incorporated into a MATLAB script to be compared with the in-house electrospray thruster, this with the goal of determining minimum arcseconds that can be achieved. Criteria of the selection for the commercially available magnetorquers and reaction wheels was limited to those that are design for use with the CubeSat platform [17-24]. For this study, a 1U CubeSat with a center of gravity located at center of the body was utilized to calculate moment of inertia I given by the following equation;

$$I = \frac{m * a}{6} \tag{3.1}$$

Where a is the distance from the center of the body to the edge of a CubeSat rail, and m is the nominal mass for a 1U CubeSat per revision 14 of the CDS. Utilizing the angular kinematic set of equations torques are utilized to calculate angular acceleration, angular velocity and angular displacement at a specified time of 1 second as described by equations 3.2, 3.3 and 3.4 respectively;

$$a_a = \frac{\tau}{I} \tag{3.2}$$

$$a_v = \omega_i + a_a * t \tag{3.3}$$

$$a_d = \theta_i + \omega_i * t + \frac{1}{2}(a_a * t^2) \tag{3.4}$$

Where τ is torque recorded, ω_i is the initial angular velocity, t is the time considered, θ_i is the initial angular position and a_a, a_v, a_d are the angular acceleration, velocity and displacement, respectively. For the case of the commercially available magnetorquers included on this study, minimum torque values available resulted inconsistent. For this, the magnetic moment of the respective magnetorquer technology was utilized to calculate achievable torque using the following equation;

$$\tau = \frac{M_m * 2 * B}{\pi} \tag{3.6}$$

Where M_m is the magnetic moment and B is the magnitude of the local magnetic force. Once all angular displacements are determined these are converted into arc-seconds using the following equation;

$$Arcseconds = a_d * 3600 \tag{3.7}$$

Following the same process, an embedded electrospray thruster with a nominal thrust of 8 μN was utilized to generate a plot in which the minimum achievable arcseconds from the thruster and the rest of the commercially available reaction wheels and magnetorquers is compared against torque. As shown in figure 9, the embedded electrospray thruster achieves the smallest value of 0.015 arcseconds, followed by the magnetorquers and reaction wheels achieving the largest value of arcseconds per 1 second of consideration.

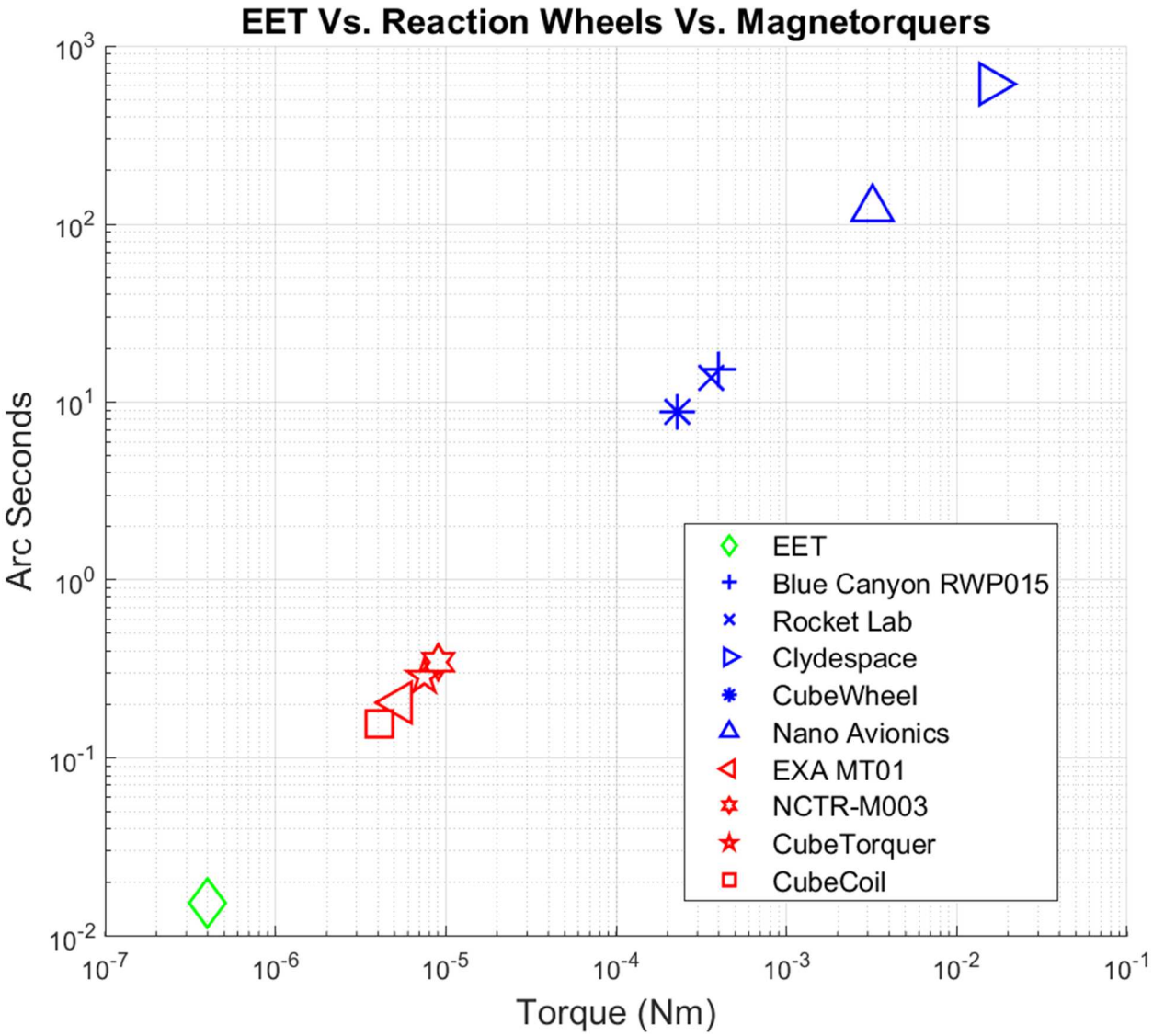

Figure 9 Pointing Accuracy Study for EET, Reaction Wheels and Magnetorquers.

Quantifying the pointing accuracy, the electrospray propulsion system is capable of achieving prompted the survey of current application given known or speculated performance parameters. For instance, a publication by John Hopkins Applied Physics Laboratory conducted an investigation into necessary accuracy for optical communication applications in spacecraft [25].

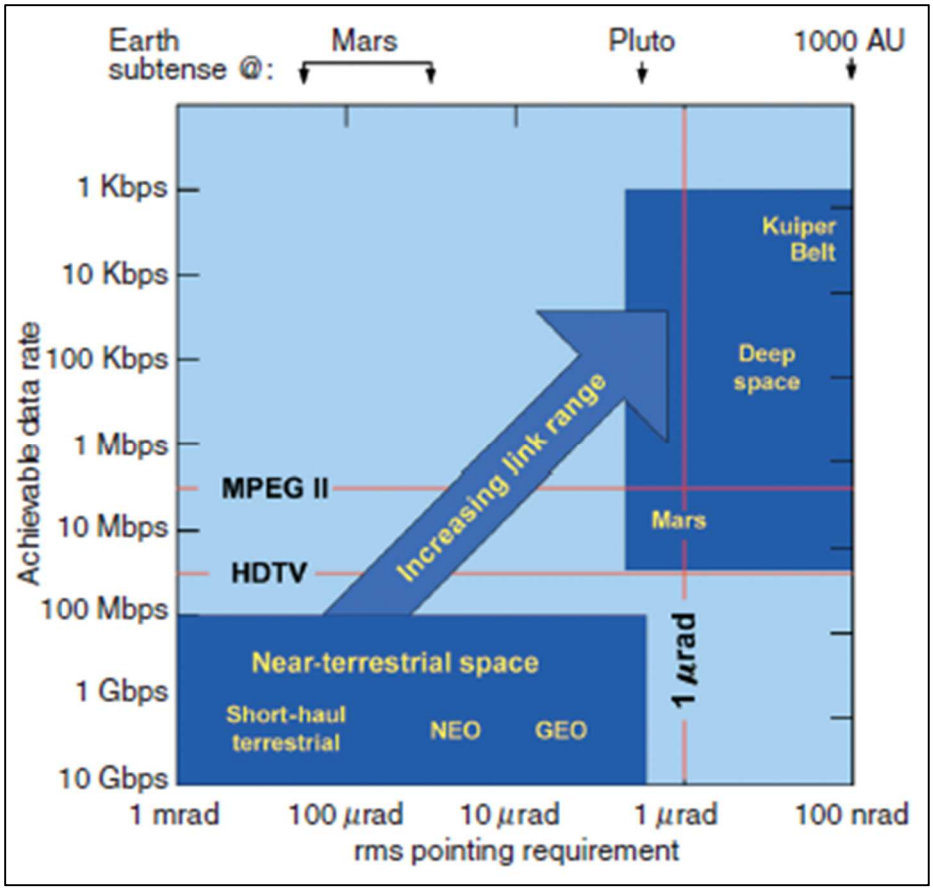

Figure 10 Communications (data rate) and pointing and tracking (rms) accuracy requirements for optical communications to increase link range for a fixed transmitted power [25].

The study compared the pointing requirements with respect of achievable data rate in which applications LEO, NEO, GEO, interplanetary including Mars and Pluto, and deep space including Kuiper Belt. Rms pointing requirements for this study ranges from 1 mrad to 100 nrad. Given the EET results from the pointing accuracy study, 0.015 arcseconds when converted to the metric use in APL's study for pointing requirement, yields about 73 nrad, which encompasses most of the categories included on figure 10 with the exception of the very distant deep space destinations

Chapter 4 STK Scenarios

4.1 LEO Maintenance Study

As discussed on Chapter 2, a platform design utilizing a 1U CubeSat was investigated to integrate an electrospray rail thruster while avoiding volume penalties. At present, LEO continues to densify as becomes more crowed and complex for mission architecture do to the steady increase of undesired space debris, satellite constellations, among others. Utilizing Ansys's Systems tool kit software (STK), a mission scenario was constructed to study the capabilities of the electrospray rail thruster for extending the operational life of CubeSats in LEO by conducting a series of periodical burn maneuvers along the velocity vector to provide the necessary ΔV in order to remain on the same orbit altitude (given some tolerances) until the satellite runs out of fuel. For this scenario, the mass and volume of a 1U CubeSat was utilized as part of the initial parameters included in the study, as shown on table 2.

Table 2 LEO Orbit Maintenance Spacecraft Parameters

Parameters	**Unit**	**1U No Propulsion**	**1U Rail Thruster**
Drag Coefficient (Cd)	-	2.2	2.2
Solar Reflection Coefficient (Cr)	-	1	1
Drag Area	m^2	0.01	0.01
Area Exposed to Sun	m^2	0.01	0.01
Satellite Total Mass	kg	1.333	1.333
Tank volume	m^3	N/A	0.000019197
Fuel Density	kg/m^3	N/A	1240
Maximum Fuel Mass	kg	N/A	0.0238
Satellite Dry Mass	kg	N/A	1.3092
Tank volume	m^3	N/A	0.000019197

To represent an electrospray rail thruster array on STK, a digital engine model with constant thrust and specific impulse was created within STK with the input parameters shown on table 3.

Table 3 STK Digital Engine model

Parameter	**Unit**	**Value**
Specific Impulse	s	1600
Thrust	μN	48
Gravity	m/s^2	9.81

To create a baseline in order to compare the extended operational life of the CubeSat, two types of scenarios were created in which initial orbital parameters, initial epoch time and spacecraft parameters remained same with the exception of 1U CubeSat utilizing the electrospray propulsion system, and the other 1U CubeSat left without a propulsion system, which would result in its orbit propagation to extend until naturally deorbiting into the atmosphere.

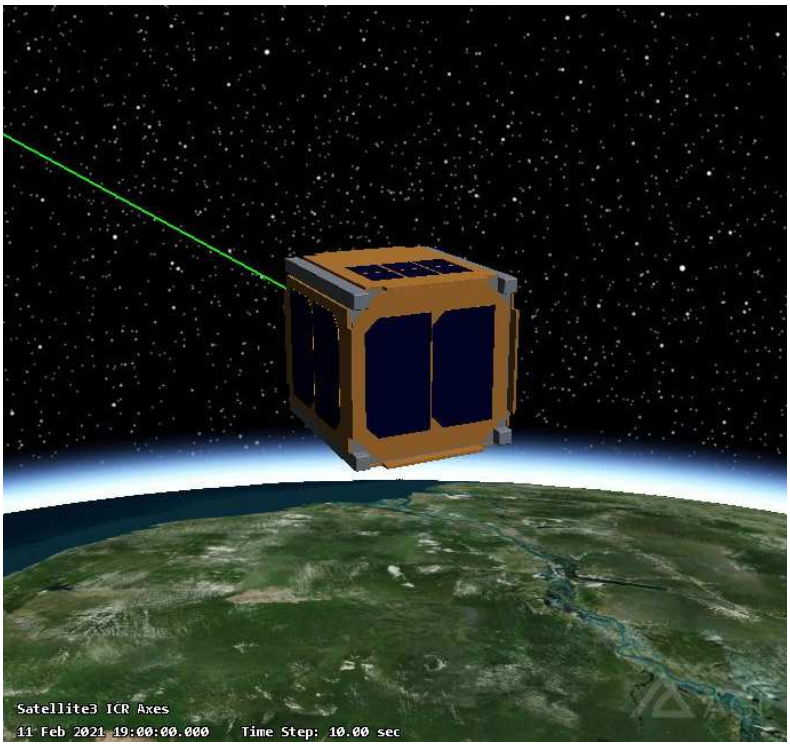

Figure 11 Simulated 1U CubeSat Model in Orbit (STK 3D Graphics Window)

Both propulsion and no-propulsion CubeSats scenarios were repeated for a total of 5 times, with the initial orbital altitude being changed in order to study 5 different types of altitudes in LEO which correspond to 250km, 300km, 350km, 450km and 500km. Inside STK lifetime tool, the Jacchia 1971 was selected as the default atmospheric model since in contains records of earth's atmospheric characteristics from the past several decades, which will become handy when taking into account different orbital periods. In an effort to consider major environmental conditions the CubeSat would experience in LEO, the initial date and time for the propulsion and no-propulsion 1Us was selected to overlap a solar maxima period in which, drag forces from Earth's atmosphere would be at the highest. On the contrary, the study was then repeated with an initial date and time selected to overlap a solar minimum at which the drag forces experienced by the spacecraft would be at its lowest. Both initial time and date parameters for the solar maxima and minima have been retrieved from NOAA's space weather prediction center, under the solar cycle progression section [26]. Using the target sequencer STK tool (described in appendix), altitude tolerances were set to simulate the 1U CubeSat performing station keeping maneuvers. The target sequencer followed a maximum and minimum altitude threshold and certain results parameters to perform this station keeping maneuver until the satellite ran of its available fuel mass.

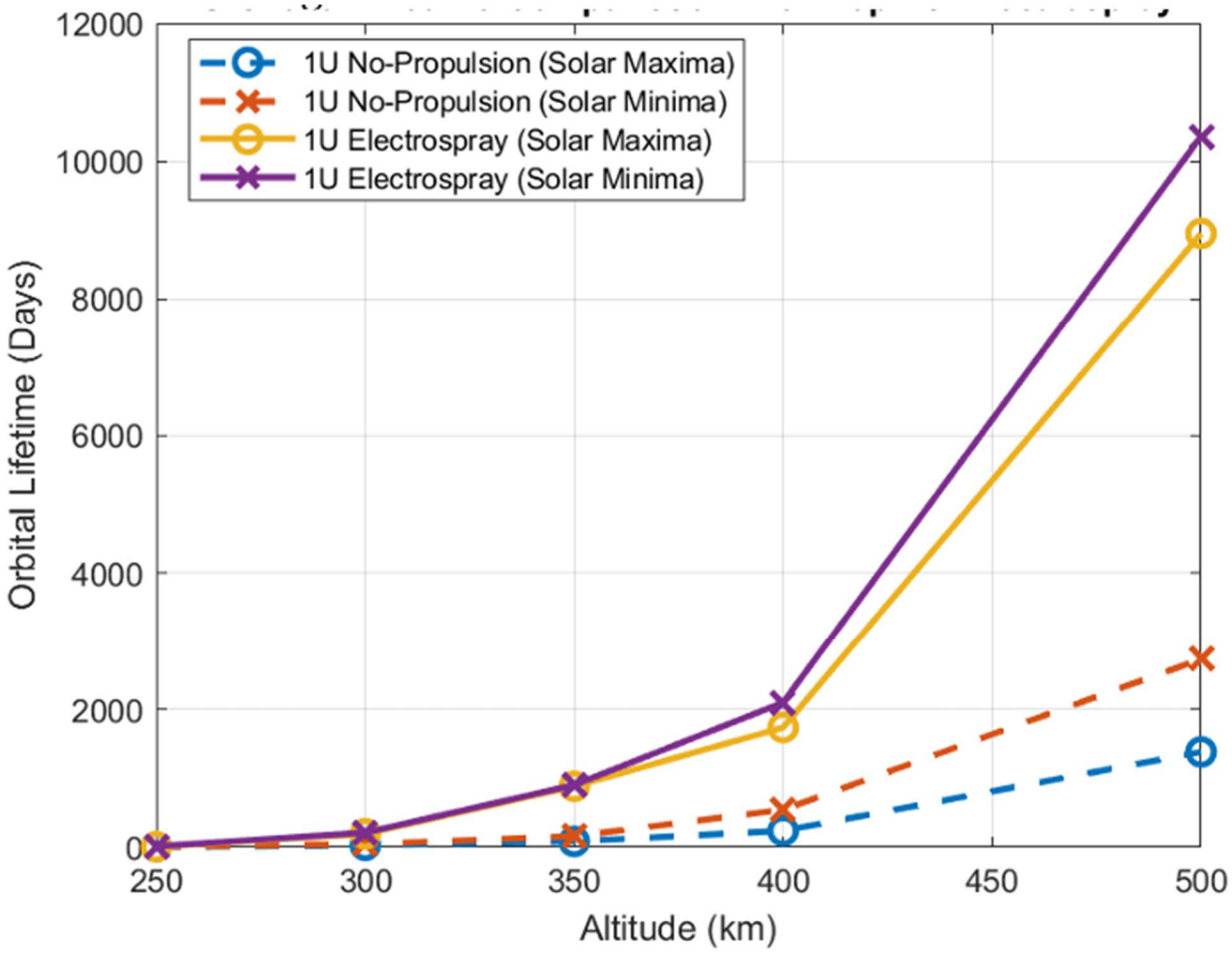

Figure 12 Propulsion Vs No Prolusion Study with Solar Maxima and Solar Minima Orbital Periods.

A MATLAB script was created in which, the total operational life for the 1U CubeSat with no propulsion and propulsion was compared and plotted for a total of 5 different initial orbits during a solar maxima and solar minima period (see figure 12). It was observed that during a solar minima period, the electrospray propulsion system can increase the operational life of a standard 1U CubeSat by 166 days at 300km, 746 days at 350 km and 1557 days (4.1 years) at 400km. In the case of the solar maxima period, the electrospray rail thruster extends the operational life of a standard 1U CubeSat by168 days at 300km, 800 days (2.2 years) at 350 km, and 1500 days (4.1 years) at 400km. It's important to note that for both solar periods the results for 500km exceed

the orbital life extension up to 20 years which, for a in high LEO which exceeds the expected operational life of a satellite this size. In the case of the smallest altitude studied (250 km) increase in operational life resulted in 1.2 days and 4.6 days for the solar maxima and solar minima period, respect. For this altitude, the electrospray propulsion system can't overcome the atmospheric drag forces thus, deorbiting before being able to utilize all of its available fuel to perform the necessary station keeping maneuvers.

4.2 GEO TO GRAVEYARD ORBIT

As more nations and private industry advance and mature their own space agencies and companies, Earth's space domain continues to become a more volatile and dense territory for satellites and spacecraft. In order to maintain the space domain accessible and available for anyone to conduct research, presence infrastructure, space tourism, communication infrastructure, among others, proper spacecraft disposal rules and guidelines must be acknowledged and meticulously followed by whoever decides to participate in the utilization of the space domain. Throughout the space domain, certain orbits around the orbit can provide advantages depending of the objectives and missions of a spacecraft or satellite. Geosynchronous orbits (GEO) in particular, have become significantly crowded over the past decades due to the demand of more advance and capable satellites in order to provide communications and conduct surveillance [27]. GEO provides an excellent opportunity fort these types of satellites since it allows the spacecraft to have an uninterrupted fixed view to earth which is achieved by matching Earth's rotation with the spacecraft's rotation around the Earth at an altitude of approximately 35,000 km. Among the set of rules guidelines that must be followed in space, non-operational spacecraft disposal can become more complex for satellites in GEO in contrast with satellites

who orbit in LEO. Drag caused by the very faint (but significant) atmosphere present in LEO, constantly trying to slow down satellites until they fully deorbit and disintegrate during atmosphere reentry. This particular feature allows mission architects to plan in advance and estimate a satellite's operational lifetime and disposal. In the case of satellites orbiting GEO, natural de-orbit of the spacecraft become not-feasible as the earth's gravitational pull becomes weaker the further away a mass is from its center, with the help of station keeping maneuvers GEO satellites can remain in orbit for outstanding periods of time. Attempting to de-orbit a satellite from GEO may be possible although significant undesirable design choices such as, dedicated de-orbit propulsion systems, increase in propellant mass and reduction in allowable payload mass, increase in power consumption, among others, must be investigated in order to integrate and carry out such maneuvers. For this, alternatives to the orbital disposal of GEO satellites have been investigated and determine, in order to maintain GEO clean and free of threats for any other user. The inter-Agency Space Debris Coordination Committee (IADC) is an international organization with the primary purpose of coordinate efforts and research related to in space debris. Whitin IADC's Space Debris Mitigation Guidelines revision 3, the concept of graveyard orbits is introduced and defined [28]. According to this guidelines Graveyard orbit for a specific spacecraft can be determined using the following equation:

$$\Delta H = 235 + (1000 * Cr * \frac{A}{m}) \tag{4.1}$$

Where ΔH is the minimum increase in perigee altitude, Cr is the Solar flux coefficient, A is the spacecraft surface area and m satellite's mass. Once ΔH is obtained, this altitude is then added to the initial GEO altitude of the satellite, yielding the final graveyard orbit. Utilizing STK, a scenario was created with the purpose of investigating a propulsion maneuver in which a 6U CubeSat with an integrated electrospray propulsion system and initial GEO orbit achieves its

respective graveyard orbit within a window of time of 15 years. As already detailed by the previous STK scenario presented, the set of electrospray thrusters are represented by the utilizing a digital engine model with constant specific impulse and thrust (see table 3).

Table 4 GEO To Graveyard Scenario Digital Engine

Parameter	**Unit**	**Value**
Gravity	m/s^2	9.81
Specific Impulse (Isp)	s	1600
Combined Thrust	μN	96

The burn maneuver plan for this scenario aims to provide linear thrust along the positive velocity vector of the satellite. For this it is assumed that the 6U CubeSat is integrated with a total of 8 electrospray thrusters on one of the rear 2U faces of a 6U CubeSat.

Table 5 Geo to Graveyard STK Scenario: Initial Orbit and Spacecraft Parameters

Parameter	**Unit**	**Value**
Altitude of Apogee	km	35786
Altitude of Perigee	km	35786
Eccentricity	-	0
Inclination	°	0
Dry Mass	kg	11.97
Drag Coefficient (Cd)	-	1
Solar Radiation Pressure (Cr)	-	1
Radiation Pressure (Ck)	-	1
Max Propellant Mass	kg	0.0238

Fuel Density	kg/m^3	1240

As described by table 4, the 6U CubeSat is set to have an initial orbit of 35,786 km. By utilizing equation 4.1 the minimum perigee altitude yields to 236.6 km thus, yielding a final graveyard orbit of 36, 022 km. In order to fully utilized the window 15 years window of time to conduct this maneuver, a set 55 periodical burns were performed with the duration of 5 hours every 0.3 years. Contrary to the LEO orbital lifetime scenario, achieving the desire orbit was determined by iterating a single planned maneuver until reaching the desire increase in altitude.

Table 6 Geo to Graveyard Scenario: Results

Name	**Unit**	**Value**
Total fuel used	g	6.05
Geo to Graveyard transfer time	yr	15
Accumulated Delta V	m/s	7.92
Burn maneuver length	hr	5
Sequencer count	-	55
Propagation time interval	yr	0.3

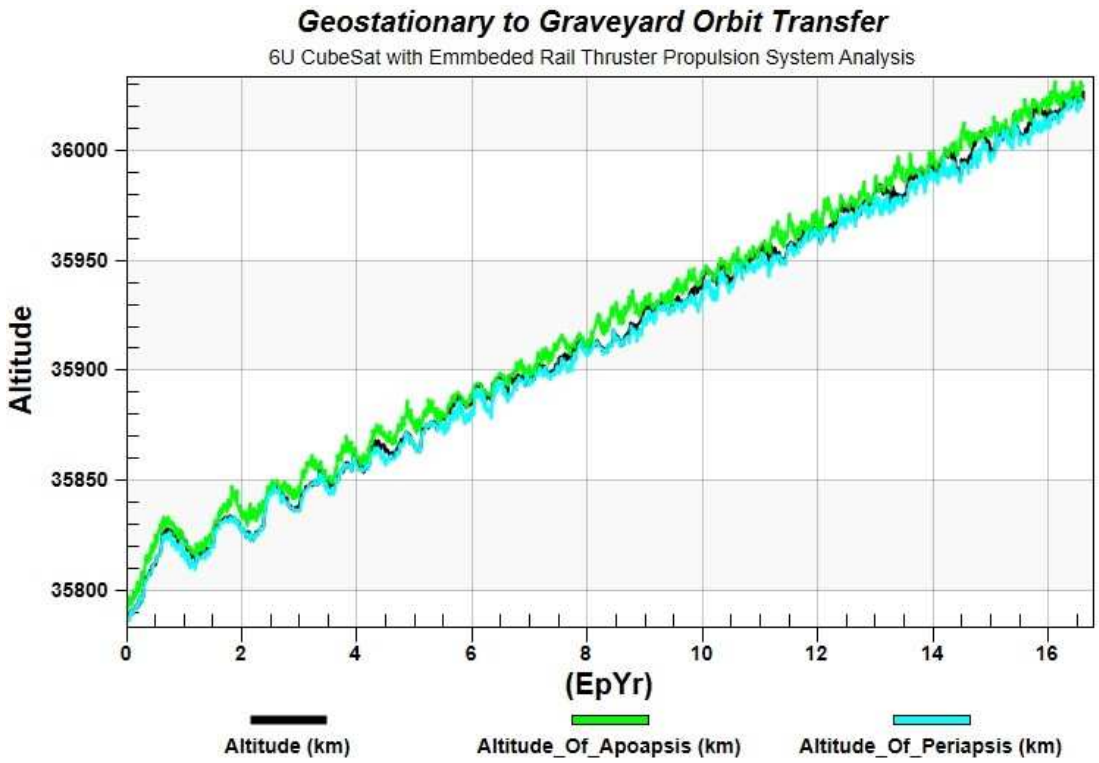

Figure 13 Geo to Graveyard Scenario: Epoch Years Vs. Altitude

Figure 13 display a plot including the geodetic altitude, altitude of apoapsis and periapsis the simulated 6U CubeSat followed during the raising orbit maneuvers. Using the Ionic liquid propellant density and volume of the total propellant tank as input parameters, after performing a total of 55 maneuvers, the spacecraft consumed a total of 6g and accumulated a total delta ΔV of 7.92 m/s. This can also be seen in figure 14, as fuel consumption increases total fuel mass decreases. It's important to note that in order to prevent eccentricity to increase as maneuvers are performed, a propagation condition was utilized to perform the 5hr burn maneuver only after reaching the current orbit apoapsis. For this study the average eccentricity remained under the order of magnitude of $1x10^{-4}$ which stands in accordance with the second condition of a graveyard orbit of having an eccentricity of equal or less than $1x10^{-3}$ according to revision 3 of IADC's Space Debris Guidelines.

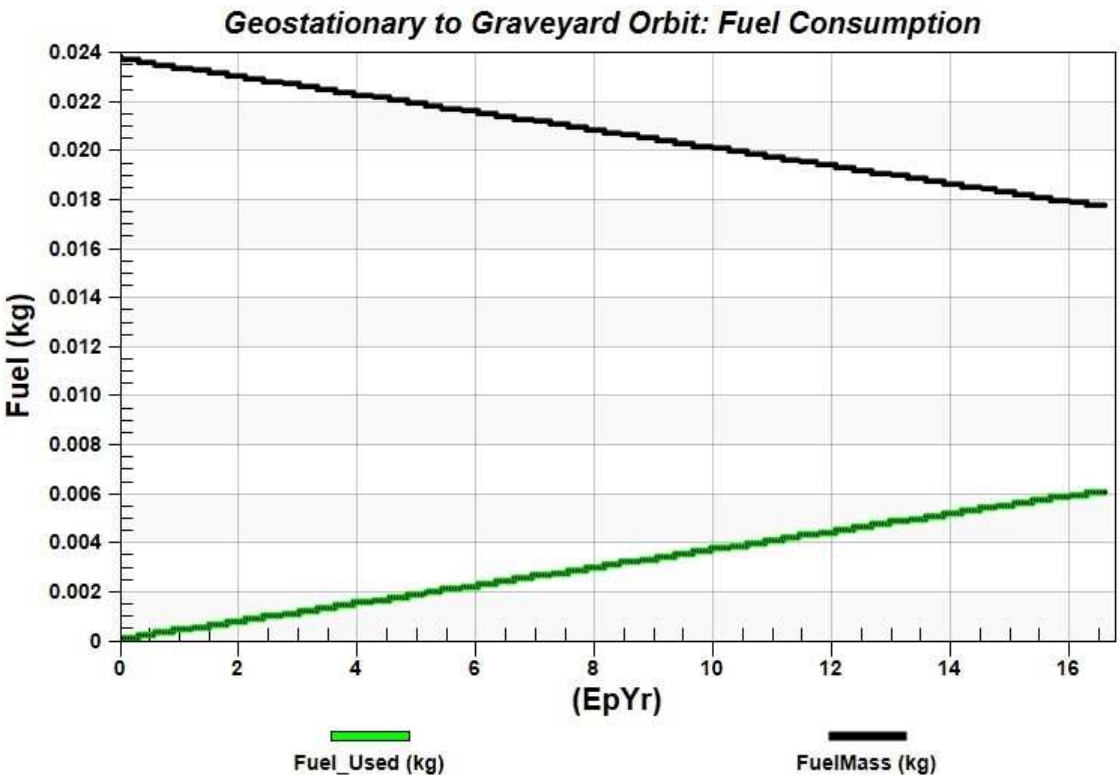

Figure 14 Geo to Graveyard Scenario: Fuel Consumption Vs. Total Fuel

Chapter 5 Conclusions & Future Work

In conclusion, the space community, industry and government entities are learning and becoming more efficient at doing more with less, when it comes to spacecraft design and mission architecture. Today, CubeSats remain as one of the most accessible platforms to reach space which is due to their low cost and simplified mission architecture integration. Over the years CubeSats have accumulated significant amounts of flight heritage in a variety of applications which include, spaceborne and Earth science observations, astrophysics, technology demonstration and in the near future, cis-lunar, interplanetary and deep space. As space missions become more demanding for small form-factor satellites, the capabilities of these platforms must be improved and extended. Traditionally, commercially available reaction wheels and magnetorquers have become the norm when it comes to integrating ADCS to CubeSats. Although these options come in a small formfactor they still occupy significant space inside the CubeSat platform that could be otherwise be used for additional payload mass and volume. Another less popular alternative to integrate an ADCS to CubeSats would be the use of propulsion systems at which these options become even less due to size and increase in complexity. The needs and challenges stated have driven the motivation to investigate an electrospray propulsion system that could integrated into the CubeSat platform without adding any SWAP penalties. Utilizing the thruster design investigated by the UTEP's Aerospace center, a 1U CubeSat structure was designed to house a total of 12 electrospray thrusters to enable a total of 6 degrees of freedom. Main features of this design can be seen in the inclusion of a fuel tank by turning the inside of a solid CubeSat rail hollow. To allocate every thruster, each individual rail is only allowed to utilize a single rail, this with the purpose of allowing every propellant tank to be independent from each other. Each thruster is also embedded into the rail in

order to avoid clearance issues for standardized P-PODs deployment mechanisms according to CDS latest revision. A pointing accuracy study was conducted in which commercially available reaction wheels and magnetorquers were compared to a single electrospray thruster, this with the goal of determining the minimal arcsecond achieved within a single second of operation. It was observed that a single thruster with thrust of 8 □N, achieves the lowest arcsecond value after 1 second of operation in comparison with the rest of the technologies included in this study. The previous motivations discussed have also prompted the creation and investigation series using STK in order to determine potential applications of the thruster and platform in orbit. The first of these scenarios aimed to extended the operational lifetime of a CubeSat in LEO by providing ΔV along the positive velocity vector to contra rest the atmospheric drag and remain in position until running out of fuel. This study was performed identically for a standard 1U CubeSat with and without propulsion, during a defined solar maxima and solar minima period in order to account for more environmental parameters experienced in LEO. Among the results, it is estimated that a 1U standard CubeSat can experience an additional increase of 20 years at the highest altitude studied (500 km) and just 1.2 days increases at the lowest altitude studied (250 km). The second STK scenario investigated the ability to perform an orbit change maneuver from GEO orbit to a Graveyard orbit for a 6U Cube with an integrated electrospray propulsion system. This maneuver was performed during a time window of time of 15 years in which the 6U CubeSat reached its Graveyard orbit by performing a series of 55 burn maneuvers 5 hrs. every 0.3 years. The next steps involving the development of the second-generation electrospray thruster currently referred to as the embedded electrospray thruster (EET) is to manufactured stainless steel extractor grids and porous glass emitters with the help of a Femto-second Laser system. Additionally, ongoing efforts continue to manufacture, assemble and test a micro-newton torsional thrust balance in

order to characterize the thrust generated by every array configuration planned. A design for a drop tower is being investigated with the goal of studying the effects of microgravity inside of the propellant tanks to be used for the electrospray thrusters.

References

1. Sovey, J., Rawlin, V., & Patterson, M. (1999, October). A synopsis of ion propulsion development projects in the United States-SERT I to Deep Space 1. In *35th Joint Propulsion Conference and Exhibit* (p. 2270).

2. Lev, D., Myers, R. M., Lemmer, K. M., Kolbeck, J., Koizumi, H., & Polzin, K. (2019). The technological and commercial expansion of electric propulsion. Acta Astronautica, 159, 213-227.
3. O'Reilly, D., Herdrich, G., & Kavanagh, D. F. (2021). Electric propulsion methods for small satellites: A review. Aerospace, 8(1), 22.
4. Mazouffre, S. (2016). Electric propulsion for satellites and spacecraft: established technologies and novel approaches. Plasma Sources Science and Technology, 25(3), 033002.
5. Keidar, M., Zhuang, T., Shashurin, A., Teel, G., Chiu, D., Lukas, J., ... & Brieda, L. (2014). Electric propulsion for small satellites. Plasma Physics and Controlled Fusion, 57(1), 014005.
6. Kristinsson, B. Ö. (2019). On the design of electrospray emitters and their microfluidic behavior (Doctoral dissertation, Massachusetts Institute of Technology).
7. Taylor, G. (1964). Electrospray. In Proceedings of Royal Society of London, London (Vol. 280, pp. 383-387). Copyright by © 2007 Cambridge University Press.
8. Guerrero, I., Bocanegra, R., Higuera, F. J., & De La Mora, J. F. (2007). Ion evaporation from Taylor cones of propylene carbonate mixed with ionic liquids. Journal of Fluid Mechanics, 591, 437-459.
9. Kulu, E. (2022, January 1). Nanosats database. Nanosats Database. Retrieved April 14, 2022, from https://www.nanosats.eu/. Copyright by © 2014 - 2022 Erik Kulu
10. CubeSat information. CubeSat. (n.d.). Retrieved April 14, 2022, from https://www.cubesat.org/cubesatinfo

11. Greig, A. D., Robali, A. B., Carrillo, C. M., & Meza, A. (2021). Design and Testing of a CubeSat Rail Integrated Electrospray Thruster. In AIAA Propulsion and Energy 2021 Forum (p. 3421).
12. Cappelletti, C., & Robson, D. (2021). CubeSat missions and applications. In Cubesat Handbook (pp. 53-65). Academic Press.
13. Pong, C. (2018). On-orbit performance & operation of the attitude & pointing control subsystems on ASTERIA.
14. Langford, A., Knapp, M., Swoboda, J., Volz, R., Erickson, P., & Lind, F. (2021). The AERO-VISTA Interactive Spectrogram (AVIS) Display: An Original Software Solution for Scientific Operations of Twin 6U CubeSats.
15. Lemmer, K. (2017). Propulsion for cubesats. Acta Astronautica, 134, 231-243.
16. Pascoa, J. C., Teixeira, O., & Filipe, G. (2018, November). A review of propulsion systems for cubesats. In ASME International Mechanical Engineering Congress and Exposition (Vol. 52002, p. V001T03A039). American Society of Mechanical Engineers.
17. Blue Canyon Technologies. (n.d.). Retrieved May 5, 2022, from https://bluecanyontech.com/components
18. Reaction wheels. Rocket Lab. (n.d.). Retrieved April 21, 2022, from https://www.rocketlabusa.com/space-systems/satellite-components/reaction-wheels/
19. Space Products & Components. AAC Clyde Space. (2021, November 11). Retrieved April 21, 2022, from https://www.aac-clyde.space/what-we-do/space-products-components
20. CubeSpace. (n.d.). Cubewheel. CubeSpace. Retrieved April 21, 2022, from https://www.cubespace.co.za/products/adcs-components/cubewheel/
21. CubeSat reaction Wheels Control System SatBus 4RW. NanoAvionics. (2022, February 3). Retrieved April 21, 2022, from https://nanoavionics.com/cubesat-components/cubesat-reaction-wheels-control-system-satbus-4rw/
22. Exa MT01 Compact Magnetorquer. CubeSatShop.com. (2021, December 29). Retrieved April 21, 2022, from https://www.cubesatshop.com/product/mt01-compact-magnetorquer/

23. NCTR-M003 magnetorquer rod. satsearch. (n.d.). Retrieved April 21, 2022, from https://satsearch.co/products/newspace-systems-nctr-m003-magnetorquer-rod
24. Cubetorquer and Cubecoil. CubeSatShop.com. (2021, March 16). Retrieved April 21, 2022, from https://www.cubesatshop.com/product/cubetorquer-and-cubecoil/
25. Boone, B. G., Bruzzi, J. R., Kluga, B. E., Millard, W. P., Fielhauer, K. B., Duncan, D. D., ... & Bokulic, R. S. (2004). Optical communications development for spacecraft applications. Johns Hopkins APL technical digest, 25(4), 306-315. Copyright by © JOHNS HOPKINS APL.
26. Solar Cycle Progression | NOAA / NWS Space Weather Prediction Center. (2004). Solar Cycle Progression | NOAA / NWS Space Weather Prediction Center. Retrieved 2022, from https://www.swpc.noaa.gov/products/solar-cycle-progression
27. Schaub, H., & Moorer, D. F. (2012). Geosynchronous large debris reorbiter: Challenges and prospects. The Journal of the Astronautical Sciences, 59(1), 161-176.
28. Inter-agency Space Debris Coordination Committee. IADC. (n.d.). Retrieved April 25, 2022, from https://www.iadc-home.org/documents_public/view/id/172#u

Appendices

APPENDIX A: MATLAB SCRIPTS

A.1 Pointing Accuracy Study: EET Vs. Reaction wheels Vs. Magnetorquers

- Determine minimum arcsecond achieved for 1 second time interval per technology category.

```
clear all
```

Constants

```
theta= 90;              % (Degrees) angle
F_t =8e-6;              % (N) thrust
L= 0.0707;              % (m) half lenght
m= 2;                   % (kg) mass
a= L*2;                 % (m) lenght
t= 1;                   % (seconds) time
Wo= 0;                  % (degrees/s) initial angular velocity
Theta_i=0;              % (degrees) Intial angle
I=(m*a)/6;              % (kg/^2) Moment of inertia of a cube
B=4.89249e-5;           % Tesla (Magnitude of Local Magnetic Force)
```

Torques compile (Thruster, Reaction Wheels, Magnetorquers)

- For rest of magnetorquers magnetic moment was utilized to calculate torque

```
% Embedded Electrospray Thruster (Nm)
T0=4e-7;            % EET
% Reaction Wheels (Nm)
T1=0.0004;          % Blue Canyon RWP015
T2=0.00036;         % Rocket Lab
T3=0.016;           % RW400 ACC Clyde Space
T4=0.00023;         % Control wheel small
T5=0.0032;          % Nano Avionics
% Magnetorquers (Nm)
T6=5.36e-6;         % Exas MT01
```

Calculations for EET

```
% Angular Acceleration from torque and moment of inertia
a_a=T0/I;                       % (degrees/sec^2)
% Angular Velocity @ system in rest initially
a_v=Wo+a_a*t;                   % (Degrees/sec)
% Angular displacement @ 1 second
```

```
a_d=Theta_i+Wo*t+(1/2)*a_a*t^2;  % (degrees)
% Arc Seconds conversion
Arc_sec= 3600*a_d;               % Arcsec
h=scatter(T0,Arc_sec,30,'greend','linewidth',1.2);
h.SizeData=200;
set(gca,'xscale','log');
set(gca,'yscale','log');
grid on
xlabel('Torque (Nm)','FontSize',14);
ylabel ('Arc Seconds','FontSize',14);
title('EET Vs. Reaction Wheels Vs. Magnetorquers','FontSize',14);
```

Calculations for Reaction Wheels

```
hold on
% Angular Acceleration from torque and moment of inertia
a_a=T1/I;      % (degrees/sec^2)
% Angular Velocity @ system in rest initially
a_v=Wo+a_a*t;       % (Degrees/sec)
% Angular displacement @ 1 second
a_d=Theta_i+Wo*t+(1/2)*a_a*t^2; % (degrees)
% Arc Seconds conversion
Arc_sec= 3600*a_d;    % Arcsec
h=scatter(T1,Arc_sec,'b+','linewidth',1.2);
h.SizeData=200;

hold on
% Angular Acceleration from torque and moment of inertia
a_a=T2/I;      % (degrees/sec^2)
% Angular Velocity @ system in rest initially
a_v=Wo+a_a*t;       % (Degrees/sec)
% Angular displacement @ 1 second
a_d=Theta_i+Wo*t+(1/2)*a_a*t^2; % (degrees)
% Arc Seconds conversion
Arc_sec= 3600*a_d;    % Arcsec
h=scatter(T2,Arc_sec,'bx','linewidth',1.2);
h.SizeData=200;

hold on
% Angular Acceleration from torque and moment of inertia
a_a=T3/I;      % (degrees/sec^2)
% Angular Velocity @ system in rest initially
a_v=Wo+a_a*t;       % (Degrees/sec)
% Angular displacement @ 1 second
a_d=Theta_i+Wo*t+(1/2)*a_a*t^2; % (degrees)
% Arc Seconds conversion
```

```
Arc_sec= 3600*a_d;    % Arcsec
h=scatter(T3,Arc_sec,'b>','linewidth',1.2);
h.SizeData=200;

hold on
% Angular Acceleration from torque and moment of inertia
a_a=T4/I;      % (degrees/sec^2)
% Angular Velocity @ system in rest initially
a_v=Wo+a_a*t;       % (Degrees/sec)
% Angular displacement @ 1 second
a_d=Theta_i+Wo*t+(1/2)*a_a*t^2; % (degrees)
% Arc Seconds conversion
Arc_sec= 3600*a_d;    % Arcsec
h=scatter(T4,Arc_sec,'b*','linewidth',1.2);
h.SizeData=200;

hold on
% Angular Acceleration from torque and moment of inertia
a_a=T5/I;      % (degrees/sec^2)
% Angular Velocity @ system in rest initially
a_v=Wo+a_a*t;       % (Degrees/sec)
% Angular displacement @ 1 second
a_d=Theta_i+Wo*t+(1/2)*a_a*t^2; % (degrees)
% Arc Seconds conversion
Arc_sec= 3600*a_d;    % Arcsec
h=scatter(T5,Arc_sec,5,'b^','linewidth',1.2);
h.SizeData=200;
```

Calculations for Magnetorquers

```
hold on
% Angular Acceleration from torque and moment of inertia
a_a=T6/I;                       % (degrees/sec^2)
% Angular Velocity @ system in rest initially
a_v=Wo+a_a*t;                   % (Degrees/sec)
% Angular displacement @ 1 second
a_d=Theta_i+Wo*t+(1/2)*a_a*t^2;  % (degrees)
% Arc Seconds conversion
Arc_sec= 3600*a_d;              % Arcsec
h=scatter(T6,Arc_sec,'r<','linewidth',1.2);
h.SizeData=200;

hold on
M_m=0.29; % Am^2 Magnetic momment of NCTR-M003 from Newspace
T7=(M_m*2*B)/pi;
% Angular Acceleration from torque and moment of inertia
```

```
a_a=T7/I;                          % (degrees/sec^2)
% Angular Velocity @ system in rest initially
a_v=Wo+a_a*t;                      % (Degrees/sec)
% Angular displacement @ 1 second
a_d=Theta_i+Wo*t+(1/2)*a_a*t^2;  % (degrees)
% Arc Seconds conversion
Arc_sec= 3600*a_d;                 % Arcsec
h=scatter(T7,Arc_sec,'rh','linewidth',1.2);
h.SizeData=200;

hold on
M_m=0.24; % Am^2 Magnetic momment of Cubetorquer
T8=(M_m*2*B)/pi;
% Angular Acceleration from torque and moment of inertia
a_a=T8/I;                          % (degrees/sec^2)
% Angular Velocity @ system in rest initially
a_v=Wo+a_a*t;                      % (Degrees/sec)
% Angular displacement @ 1 second
a_d=Theta_i+Wo*t+(1/2)*a_a*t^2;  % (degrees)
% Arc Seconds conversion
Arc_sec= 3600*a_d;                 % Arcsec
h=scatter(T8,Arc_sec,'rp','linewidth',1.2);
h.SizeData=200;

hold on
M_m=0.13; % Am^2 Magnetic momment of CubeCoil
T9=(M_m*2*B)/pi;
% Angular Acceleration from torque and moment of inertia
a_a=T9/I;                          % (degrees/sec^2)
% Angular Velocity @ system in rest initially
a_v=Wo+a_a*t;                      % (Degrees/sec)
% Angular displacement @ 1 second
a_d=Theta_i+Wo*t+(1/2)*a_a*t^2;  % (degrees)
% Arc Seconds conversion
Arc_sec= 3600*a_d;                 % Arcsec
h=scatter(T9,Arc_sec,'rs','linewidth',1.2);
h.SizeData=200;
```

Plot & Legend formatting

```
lgd=legend('EET','Blue Canyon RWP015','Rocket Lab','Clydespace', ...
    'CubeWheel','Nano Avionics','EXA MT01', ...
    'NCTR-M003','CubeTorquer','CubeCoil','location','best');

lgd.FontSize=11;
```

A.2 Solar Maxima and Solar Minima 1U No-propulsion Vs. Propulsion

- Using STK data from scenario, compared extended operational lifetimes

```
% initial altittudes for LEO
Al=[250,300,350,400,500]; % (km)

% 1U No-prop results
SMa=[9,30,87,242,1387]; % (Days) Solar Maxima
SMi=[12,48,162,547.5,2737.5]; %(Days) Solar Minima

% 1U Electrospray Thruster Results
SMa_e=[10.2,198,887,1742,8951]; % (Days) Solar Maxima
SMi_e=[16.6,214.11,907,2104.5,10362.5]; %(Days) Solar Minima

% Ploting No-prop
plot(Al,SMa)
hold on
plot(Al,SMi)

% Ploting Electrospray Rail-thuster
plot(Al,SMa_e)
plot(Al,SMi_e)
```

APPENDIX B: STK SCENARIOS SET-UP

B.1 LEO Operational Life Study

The schematic shown in figure 7 illustrates the analysis plan followed to perform a life expectancy comparison between the electrospray integrated 1U CubeSat and 1U CubeSat without propulsion system. To avoid unnecessary complexity in the study, the orbits for both CubeSats have been limited to Low earth orbit, and the end of operational life parameter was selected to be an arbitrary altitude value for the CubeSats. Since the low earth orbit's atmosphere's density is significant, it imparts drag on satellites causing them to lose altitude with

respect to time. For this matter, a satellite with an integrated propulsion system can aid to extend the satellites lifetime by periodically raising the orbit of the satellite until running out of fuel.

As the previous analysis carried, a single STK scenario is created after which two satellites are inserted with the "define properties" option. Starting with the satellite featuring no propulsion, the astrogator is selected as the propagator and an arbitrary initial orbit is defined, it is important to note that in order for the analysis to be able to provide a meaningful comparison, both initial

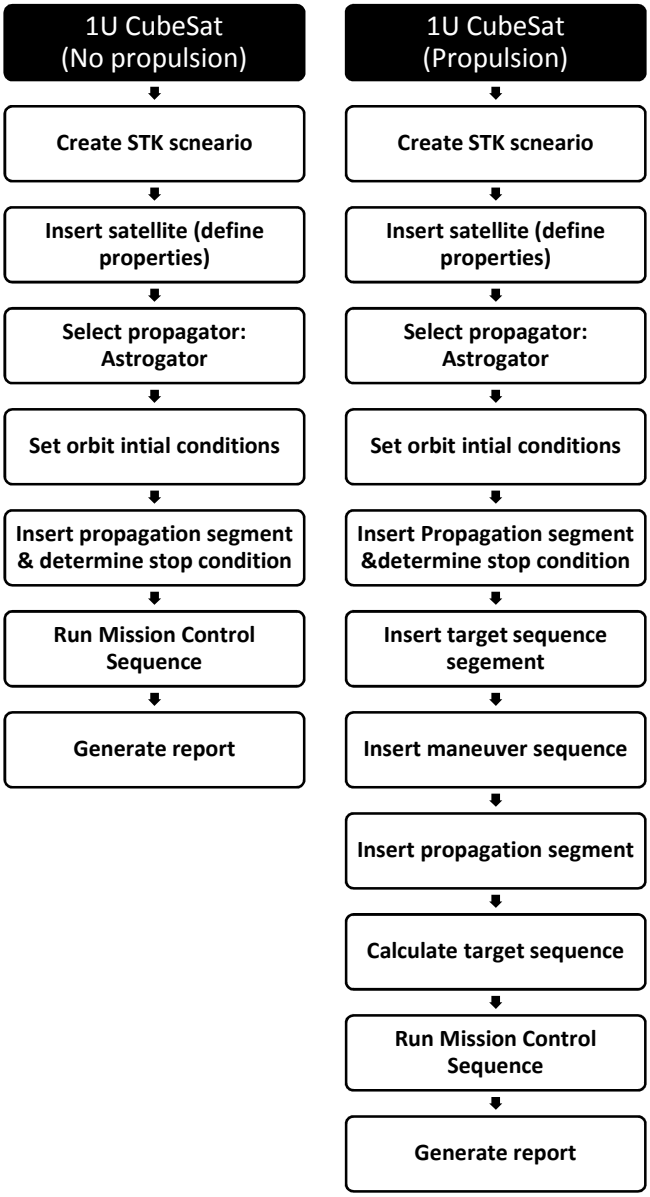

Figure 7: Analysis schematic summary for satellite lifetime impact

orbit parameters and conditions for the satellites must remain the same. This will allow an easier and more direct comparison between the impacts of including and not including a propulsion system for a satellite orbiting in low Earth orbit. Next, a propagation segment is inserted after the initial conditions segments and the stopping condition defined as an altitude threshold. Reports and graphs can be accessed and generated by right clicking on the satellite's name located on the object browser.

Moving on with the satellite featuring the electrospray propulsion system, the steps following to the insertion of the propagation segment will remain the same, to allow a fair comparison between the two spacecrafts. A target sequence segment is inserted after the first propagation segment and the profile is set to differential corrector.

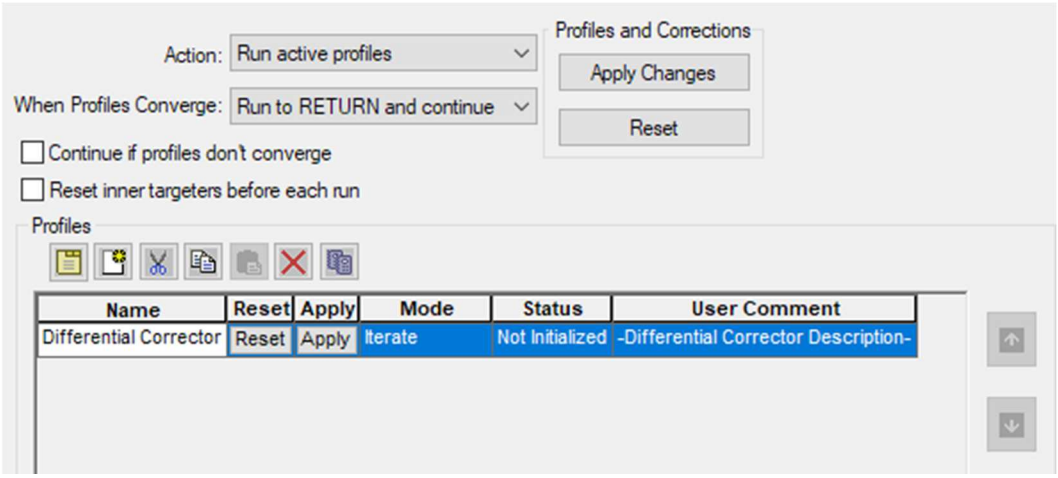

Figure 8: Target sequence window

As performed on the previous performance analysis for the satellite's dynamics, the electrospray thruster system will be simulated by creating a new component and manually inputting the values for specific impulse and thrust. The maneuver type is set to finite, along velocity vector and the attitude control set to "along velocity vector. Making sure the Electrospray thruster is generated, two stopping conditions are inserted on the maneuver's propagator window

corresponding to a duration stopping condition (which is selected as target control parameter and delta-V stopping condition).

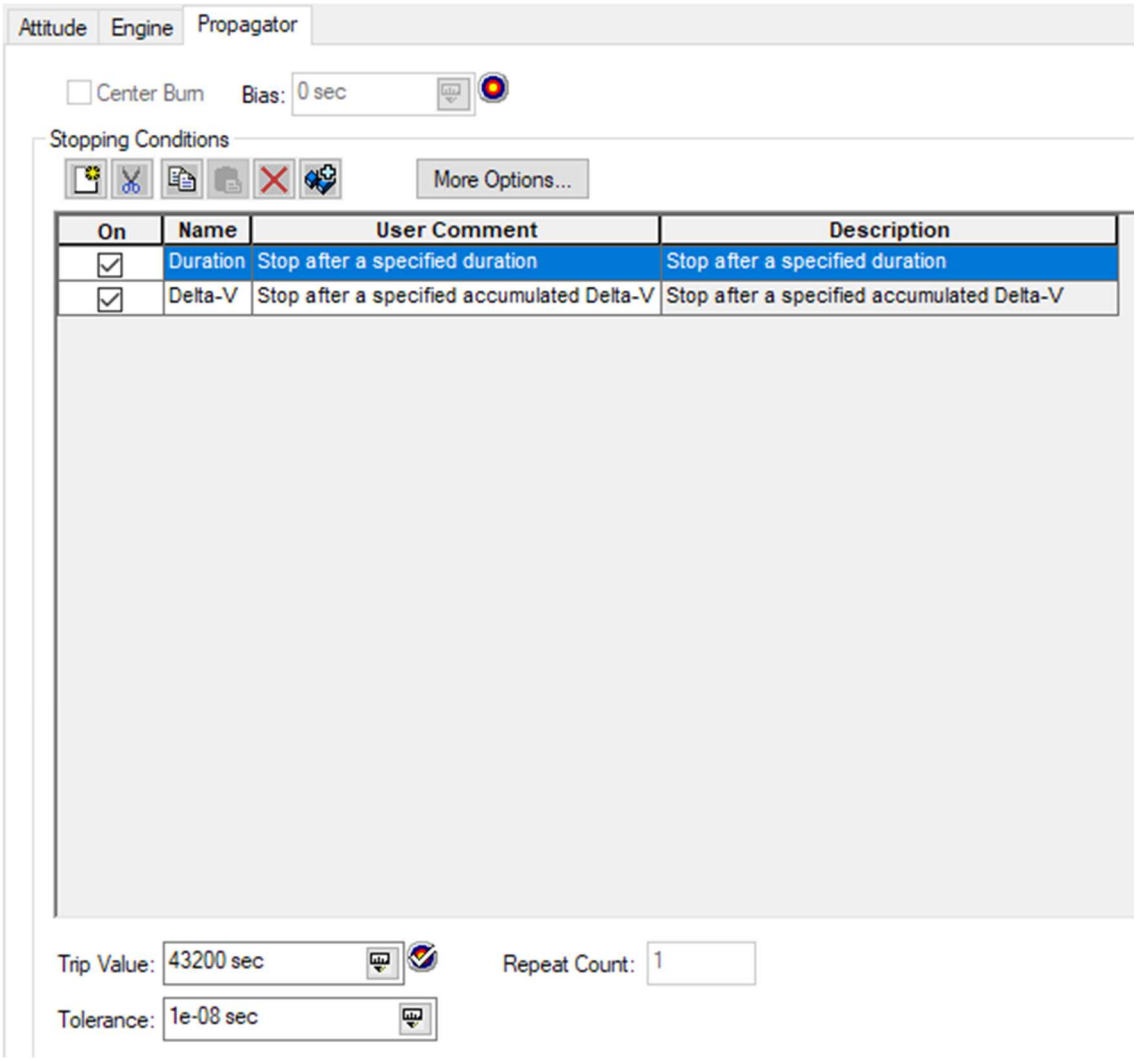

Figure 9: Maneuver's segment Propagator window

A result equality constraint is created for attitude since it will determine the desired altitude that the burn maneuver needs to achieve. Accessing the differential corrector properties will display both the control parameters and the equality constraints which are enabled and the desired altitude manually inputted.

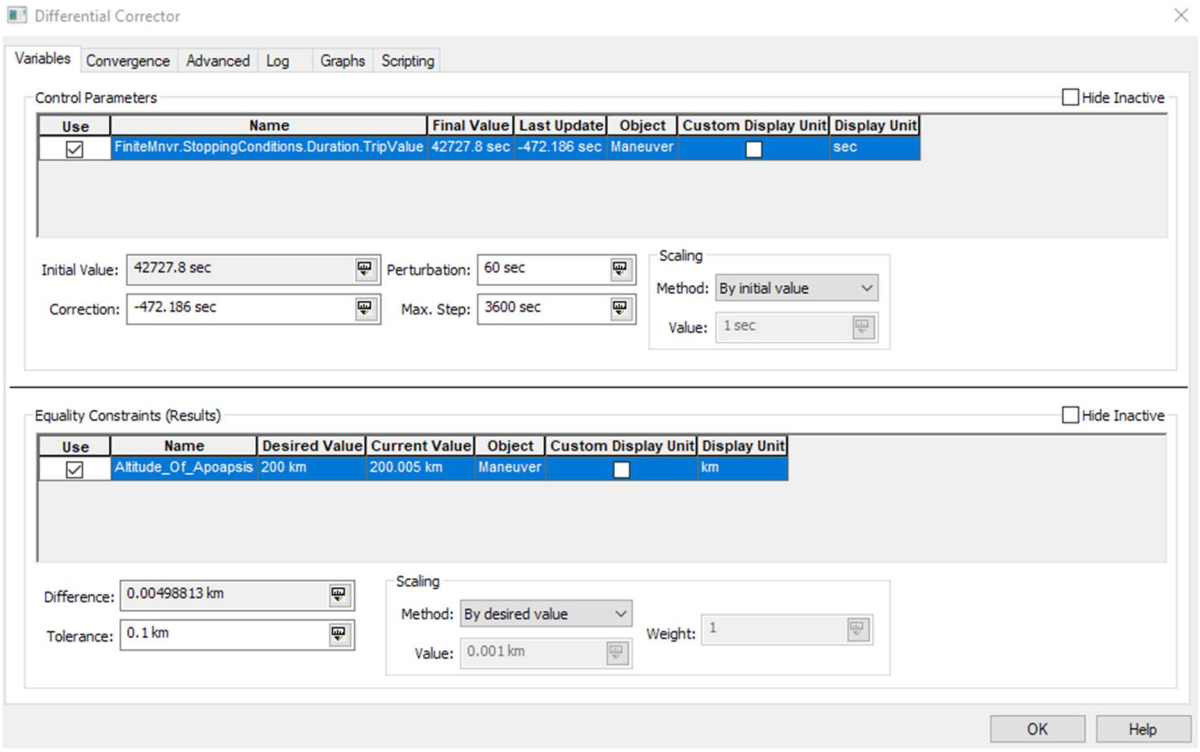

Figure 10: Differential corrector properties

The target sequence is then run along the mission control sequence while running on all active profiles. After the solution converges, the reports and graphs manager can be accessed by right clicking the satellite's name located on the object browser box.

B.2 GEO to Graveyard Orbit STK scenario Set-up

The following steps describe the steps and methodology utilized to create and run the Geo to Graveyard orbit STK scenario. At the time of this study STK 12.0.0 remained as the software version employed for the scenario.

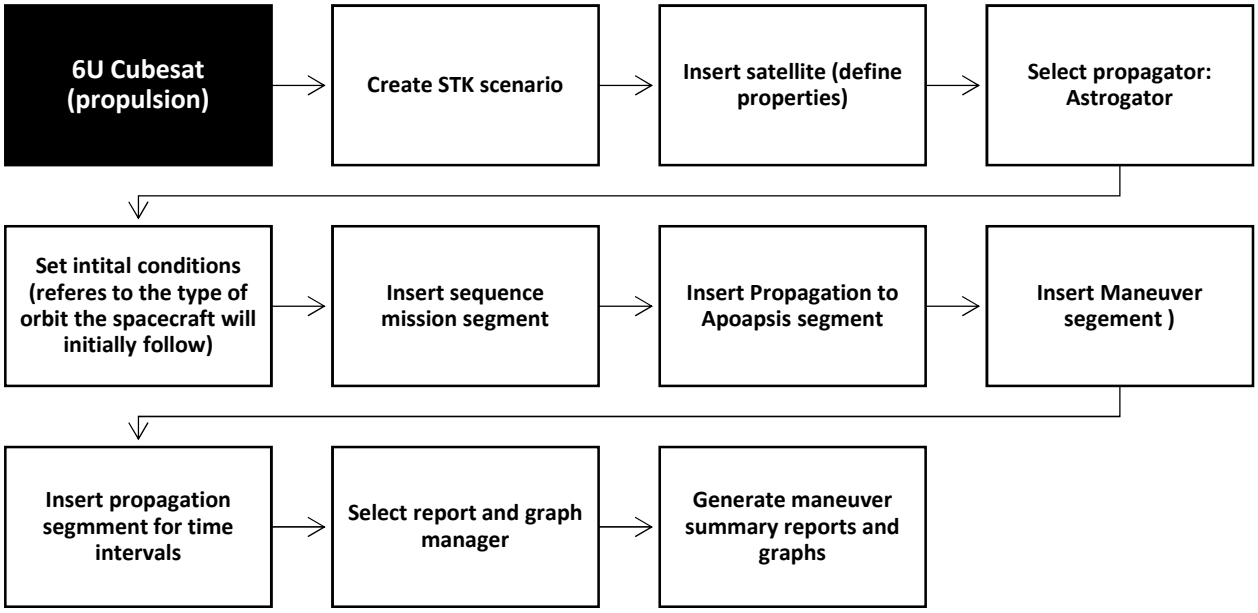

Figure 15 GEO To Graveyard Orbit set-up path

Figure 15 describes the order for the mission segments used for the study. Initial state parameters must be inputted first which encompass the spacecraft paramters and initial orbit parameter. For this study, a mission sequence segment was employed to repeat a specific set of events as necessary. This is done by including any propagation/maneuver segment underneath the sequence segment

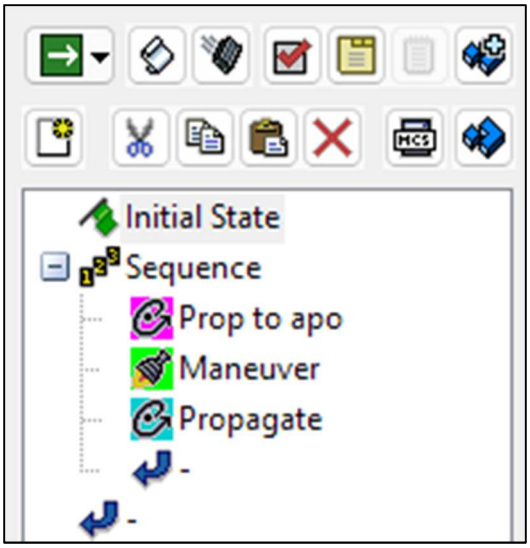

Figure 16 GEO to Graveyard Orbit Mission Sequence Segments

Inside the sequence window, the repeat count is set to 55 with the generated ephemeris checked and a final state to pass to next segment setting.

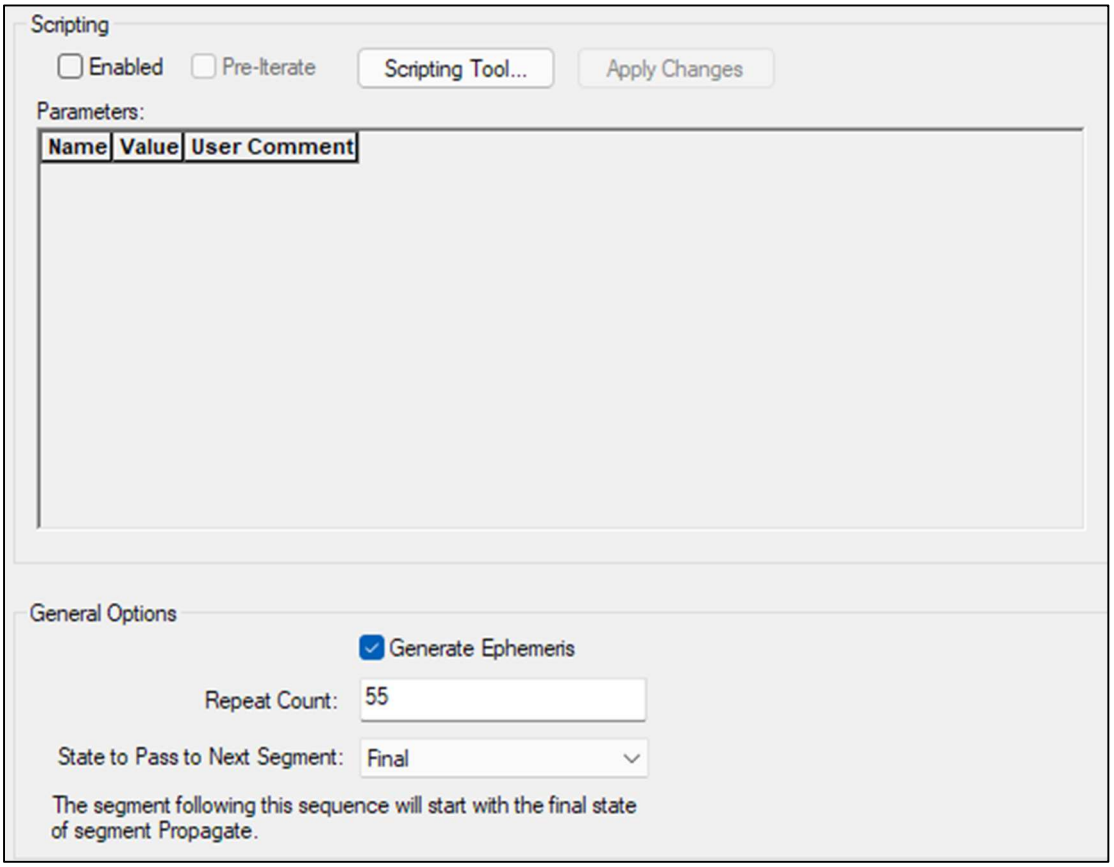

Figure 17 GEO to Graveyard Orbit Sequence Window

The first segment to follow the sequence segment will be a propagation segment with the goal of propagating the spacecraft to the current orbit apoapsis (see figure 17)

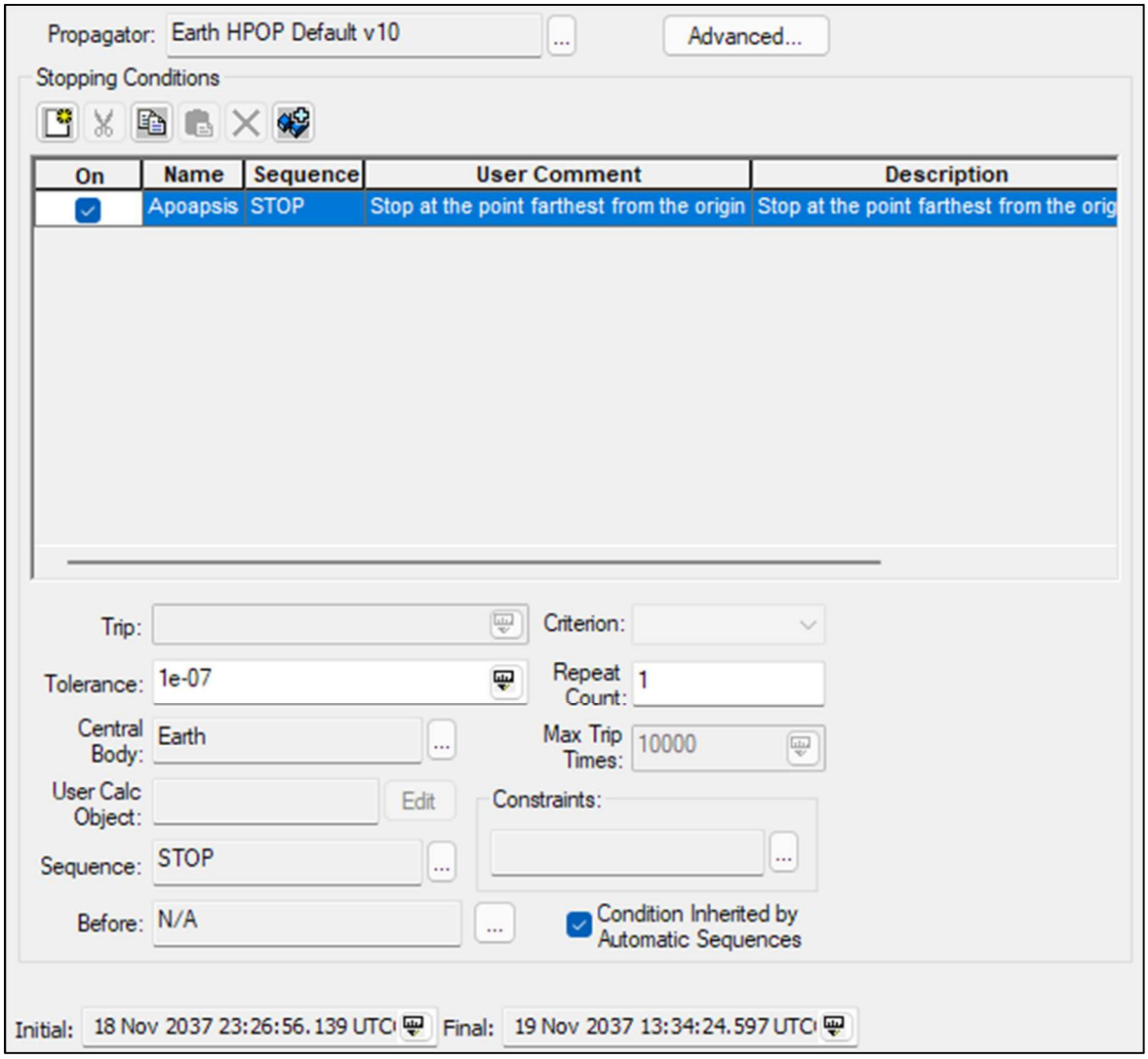

Figure 18 GEO to Graveyard Orbit Propagation to Apoapsis Segment Window

Inside the maneuver segment window, type is set to finite, force and model for optimization propagator set to EARTH HPOP Default V10. Underneath the altitude tab, attitude control is set for along velocity vector and the attitude update, to update during burn.

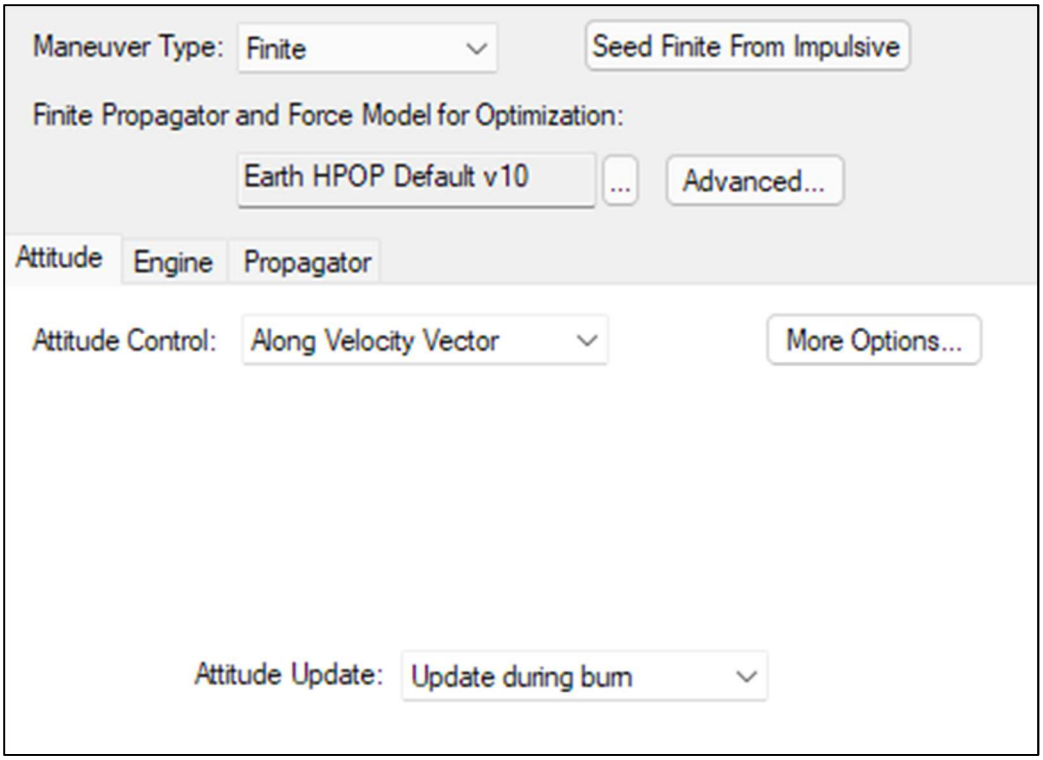

Figure 19 GEO to Graveyard Orbit Maneuver Segment Attitude Window

Underneath the engine tab, (as seen on figure19) the propulsion type is set to engine model with the digital electrospray engine model generated as the selection.

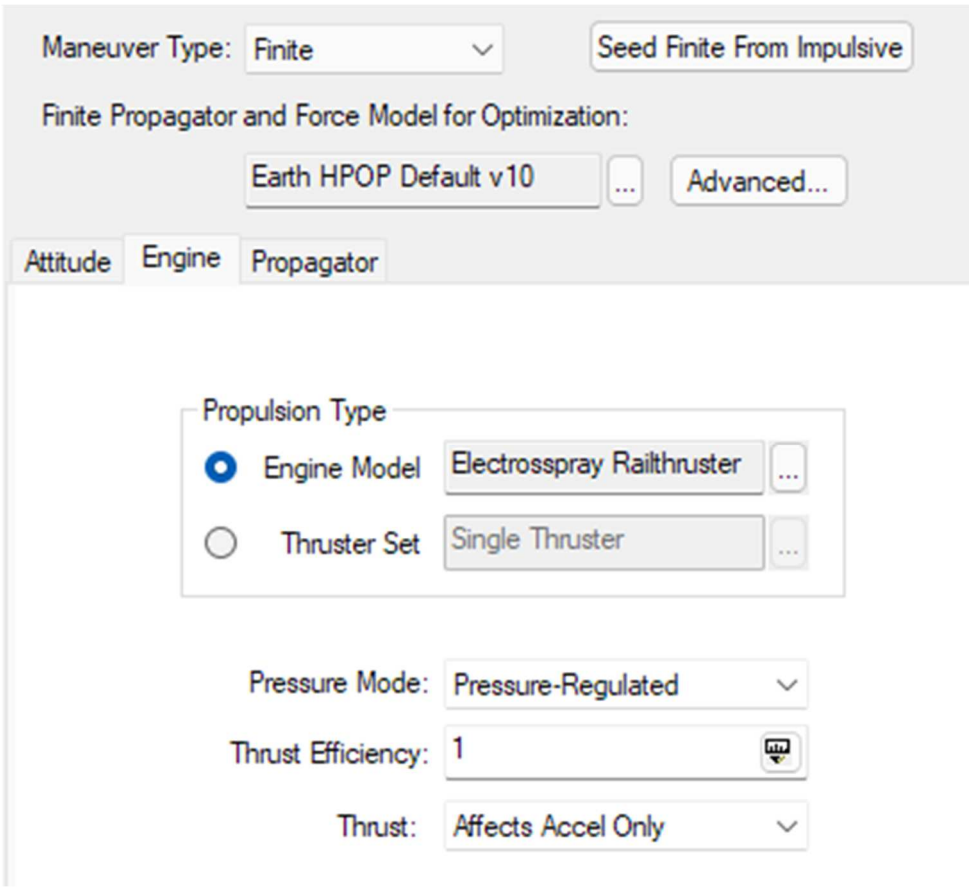

Figure 20 GEO to Graveyard Orbit Maneuver Segment Engine Window

Underneath the propagator tab for the maneuver segment, a duration stopping condition is define, this with the purpose of indicating the duration of the burn maneuver before moving to the next segment. Duration for this stopping condition is set to 1800 seconds (5 hrs). (See figure 20)

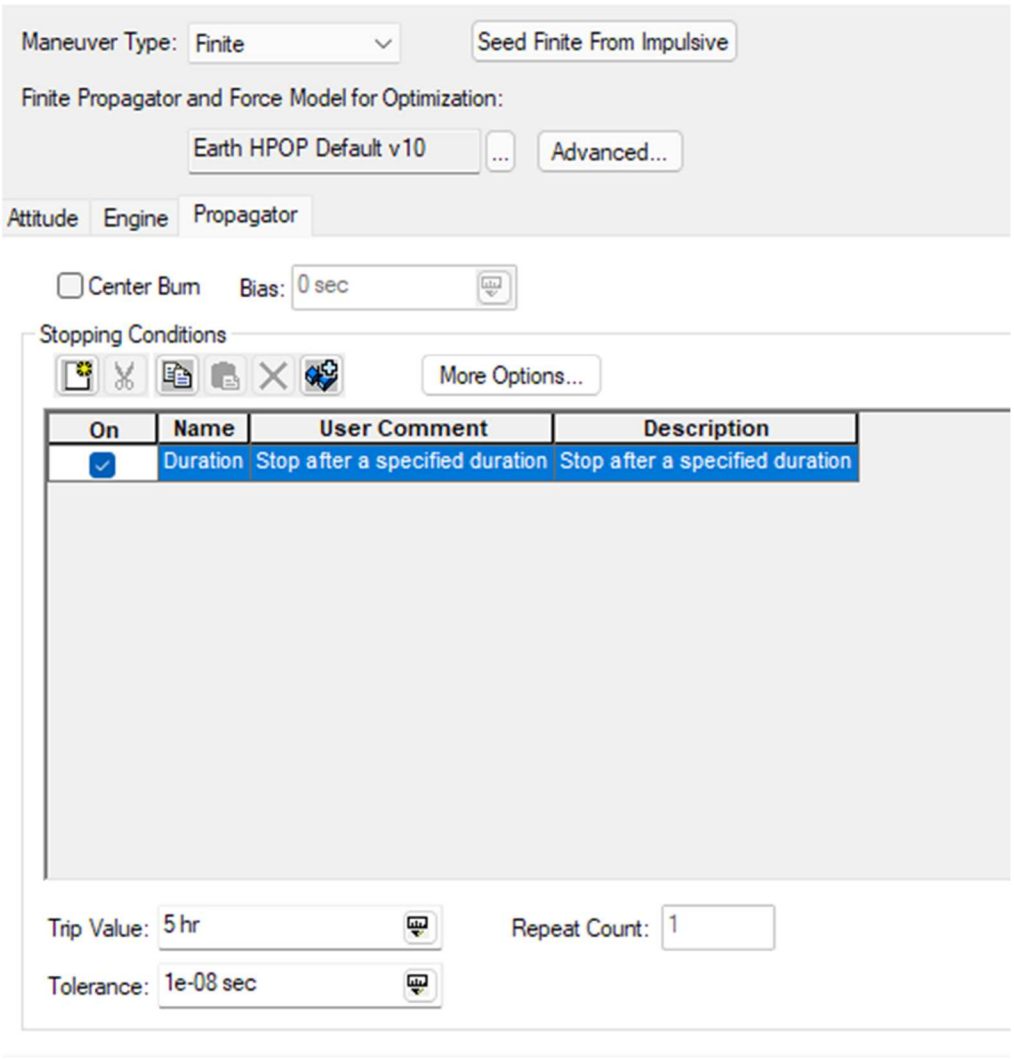

Figure 21 GEO to Graveyard Orbit Maneuver Segment Propagation Window

The last mission segment used before starting back at the top of the sequence will be another propagation segment with a duration stopping condition (see figure 21). Trip for this stopping condition is set to 0.3 which accounts for the spacecraft to coast until performing another burn maneuver.

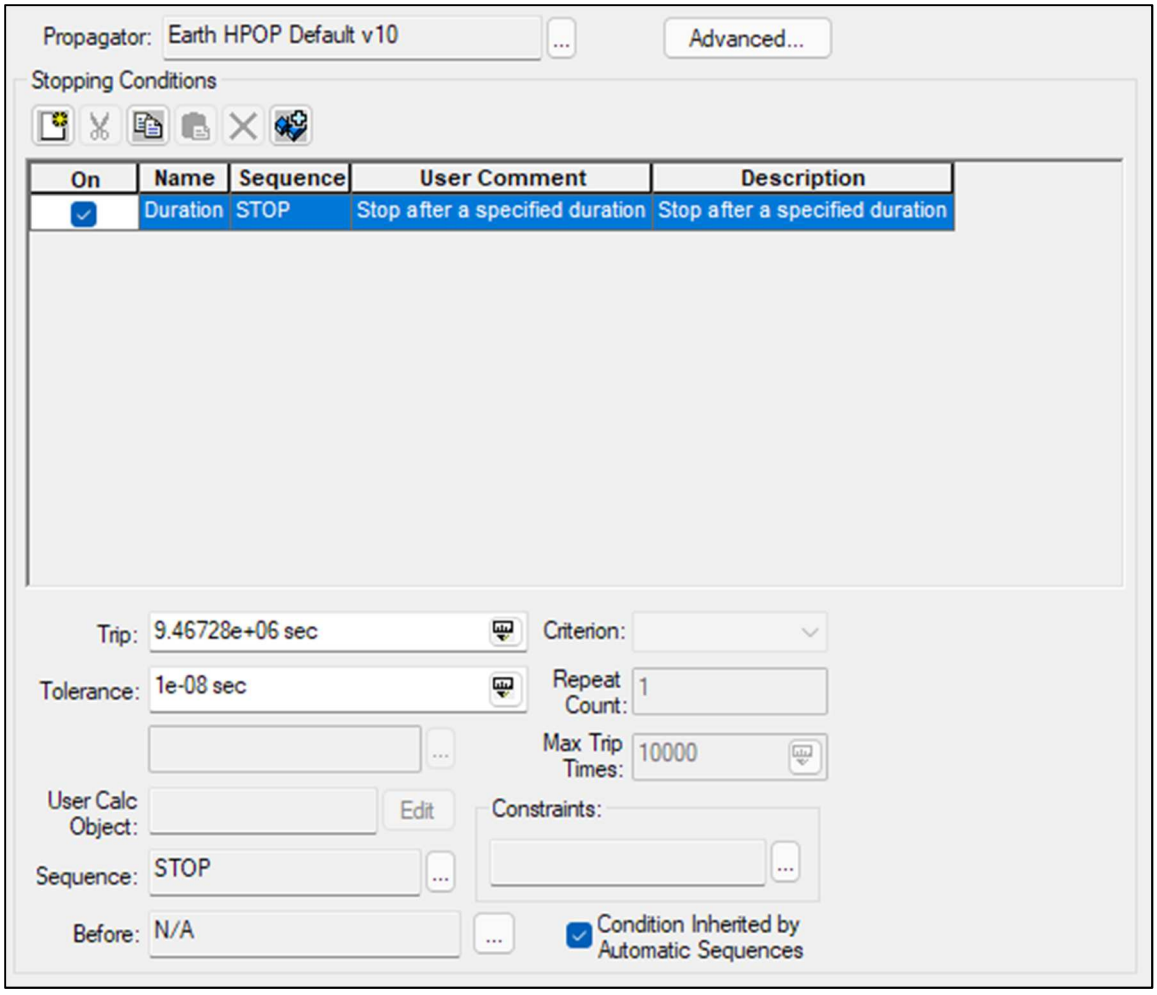

Figure 22 GEO to Graveyard Orbit Spacecraft Coast Propagation Window

Vita

Alberto Meza found interest in the STEM field trough literature in the fields of, astrophysics, biology and engineering to name a few. As an undergraduate student at the University of Texas at El Paso, he pursued a major in mechanical engineering in which then decided to get involved with UTEP's SAE Aero team as the CFD team lead for most of his undergraduate career. After earning his bachelor's degree in August 2020, he decided to pursue a Master's in Mechanical engineering after which he began his graduate studies as a graduate research assistant under the supervision of Dr. Amelia Greig at UTEP's Aerospace Center. His graduate research has revolved around propulsion systems for small satellites, which included the Electrospray propulsion project and the Cold-Gas demonstrator CubeSat. Alberto became a co-author in July 2021 at the AIAA Propulsion and Energy conference with a paper titled "Design and Testing of a CubeSat Rail Integrated Electrospray Thruster". Alberto took part of a co-op with MIT Lincoln laboratories during the fall 2022 semester in which he supported Division 7, group 71 in various projects including the AERO VISTA mission. During the spring 2022 semester, he became a co-author once again during the Southwest Emerging Technology Symposium in 2022, in which he published a paper titled "Extending In-Orbit Capabilities of CubeSats with Modular Embedded Electrospray Thrusters". Alberto earned his Master of Science in mechanical engineering in May 2022, after which took part on a summer internship with AFRL at Edwards Airforce base, working under the electrospray propulsion project.